田中　淳					
Tanaka A, Takeda S, Kariya R, Matsuda K, Urano E, Okada S, Komano J*.	A novel therapeutic molecule against HTLV-1 infection targeting provirus.	***Leukemia***			In press.
inno-Oue A, Tanaka A, Shimizu N, Mori T, Sugiura N, Kimata K, Isomura H, Hoshino H.	Inhibitory Effect of Chondroitin Sulfate Type E on the Binding Step of Human T-Cell Leukemia Virus Type 1.	***AIDS Res Hum Retroviruses.***			In press
Tanaka A, Jinno-Oue A, Shimizu N, Hoque A, Mori T, Islam S, Nakatani Y, Shinagawa M, Hoshino H.	Entry of human T-cell leukemia virus type 1 is augmented by heparin sulfate proteoglycans bearing short heparin-like structures.	***J Virol.***	86(6)	959-2969	2012
Mori T, Shimizu N, Jinno-Oue A, Tanaka A, Shinagawa M, Tokizawa S, Akagi T, Hoshino H.	Tax1-expressing feline 8C cells are useful to monitor the life cycle of human T-cell leukemia virus type I.	***J Gen Virol.***	93(Pt 3)	588-593	2012

Ⅳ. 平成２４年度　刊行物別刷（抜粋）

SCIENTIFIC REPORTS

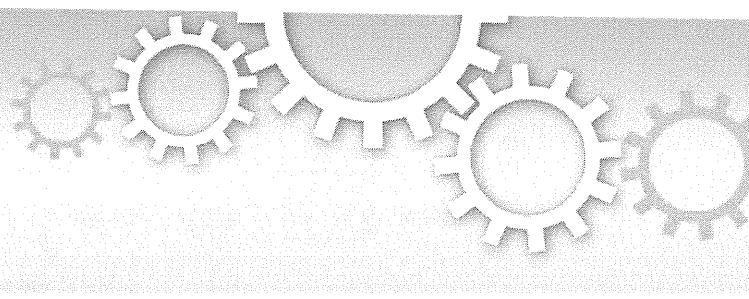

SUBJECT AREAS:
MOLECULAR ENGINEERING
GENE THERAPY
VIROLOGY
TUMOUR SUPPRESSORS

Received
30 November 2011

Accepted
12 March 2012

Published
11 April 2012

Correspondence and requests for materials should be addressed to J.K. (ajkomano@nih.go.jp; komano@iph.pref.osaka.jp)

* Current address: Research Center for Allergy and Immunology, RIKEN Yokohama Institute, 1-7-22 Suehiro-cho, Tsurumi, Yokohama, Kanagawa, 230-0045, Japan.

#Current address: Osaka Prefectural Institute of Public Health, Dept. Of Infectious Diseases, 3-69, Nakamachi, 1-chome Higashinari-ku, Osaka, 537-0025, Japan.

Therapeutic potential of HIV protease-activable CASP3

Kosuke Miyauchi*, Emiko Urano, Mari Takizawa, Reiko Ichikawa & Jun Komano#

AIDS Research Center, National Institute of Infectious Diseases, 1-23-1 Toyama, Shinjuku-ku, Tokyo 162-8640, Japan.

Development of a therapeutic application of CASP3/caspase 3/CPP32, an executor of apoptosis, has been challenging because regulation of its activation is complicated. This study aimed to inhibit cancer cell growth and human immunodeficiency virus type 1 (HIV-1) propagation through a CASP3 mutant, CASP3*, activable by HIV-1-encoded aspartate protease. Active CASP3* was delivered to leukemic cells using a protein transduction vehicle, the lentivirus-like nanoparticle (LENA), which should contain thousands of CASP3*-Gag protein molecules and release the activated CASP3* into the target cell cytoplasm. CASP3*-LENA induced apoptosis in various types of leukemic cells. In addition to being effective against leukemic cells, constitutive expression of CASP3* restricted HIV-1 propagation in SUP-T1 cells. The attenuation of HIV-1 replication in SUP-T1/CASP3* cells was attributed to the elimination of HIV-1-infected cells by apoptosis. These data suggest that CASP3* has therapeutic potential against both lymphoid malignancies and HIV-1 infection.

CASP3 is expressed as an inactive pro-enzyme that is activated upon exposure to apoptosis-inducing stimuli[1,2]. Pro-CASP3 undergoes proteolytic processing by CASP8, 9 and 10 that yields three polypeptides: the pro domain, p17 and p12. The p17 and p12 form a heterodimer that executes the protease activity. CASP3 activates itself as well as CASP6, 7 and 9 by proteolytic cleavage and amplification of the signal for the execution of apoptosis. The therapeutic application of CASP3 is limited because of this complex regulation[3–5]. We overcome this problem by genetic engineering the CASP3.

Here, a mutant of CASP3 designed to be activated specifically by the aspartate protease of human immunodeficiency virus type 1 (HIV-1), but not by other CASPs, was produced (CASP3*) and a proof-of-concept study was conducted to demonstrate the therapeutic potential of CASP3* against lymphoid malignancies and HIV-1 infection.

To achieve leukemic cell killing by CASP3*, a lentivirus-like nanoparticle (LENA) system was utilized[6]. The LENA system is a simple, efficient and reproducible method that we have developed to transduce proteins into mammalian cells[6]. The LENA is different from lentiviral vector in that the former system delivers proteins that are encapsidated into the nanoparticles but not genes as does the latter. Protein transduction does not require *de novo* transcription and translation, and the transferred protein functions immediately after the transduction. Also, LENA is biologically safe since LENA is not an "infectious" agent. Approximately 5,000 CASP3*-Gag proteins are packaged, processed and activated by HIV-1 protease in the particle of LENA. CASP3*-LENA, facilitated by vesicular stomatitis virus G protein (VSV-G), binds to cells and enters them via endocytosis. Membrane fusion between the cell and LENA takes place at the endosome in a VSV-G-dependent manner. The LENA content is then released into the cell cytoplasm. We expected an initiation of apoptosis in CASP3*-LENA-exposed leukemic cells immediately after membrane fusion.

In the HIV/AIDS field, clinical trials have proved that gene therapy approaches are indeed effective against HIV-1 infection[7,8]. However, the emergence of treatment-resistant viruses is problematic, since HIV-1 is a highly mutagenic virus. Also, the "off-target" effect of therapeutic molecules is a serious concern. Thus, developing a highly specific therapeutic gene against HIV-1 provides another option for treatment of HIV-1-infected individuals in a molecular therapy approach.

In this study, the genetically-engineered CASP3 activated specifically by HIV-1 protease was shown to have therapeutic potential against both lymphoid malignancies and HIV-1 infection.

Results

CASP3* has proteolytic cleavage sites for HIV-1 protease adopted from the matrix (MA or $p17^{MA}$)-capsid (CA or $p24^{CA}$) junction of HIV-1 $Pr55^{Gag}$ (Gag, Fig. 1a). The myristoylation signal of Lyn was attached at the amino-terminus and serves as a membrane-targeting signal. The pro domain of CASP3 was dispensable for enzyme activity and was removed from this construct. Then, the CASP3* was applied to the LENA system for the leukemic cell killing experiment (Fig. 1b). The CASP3*-Gag and its proteolytic products were detected in the

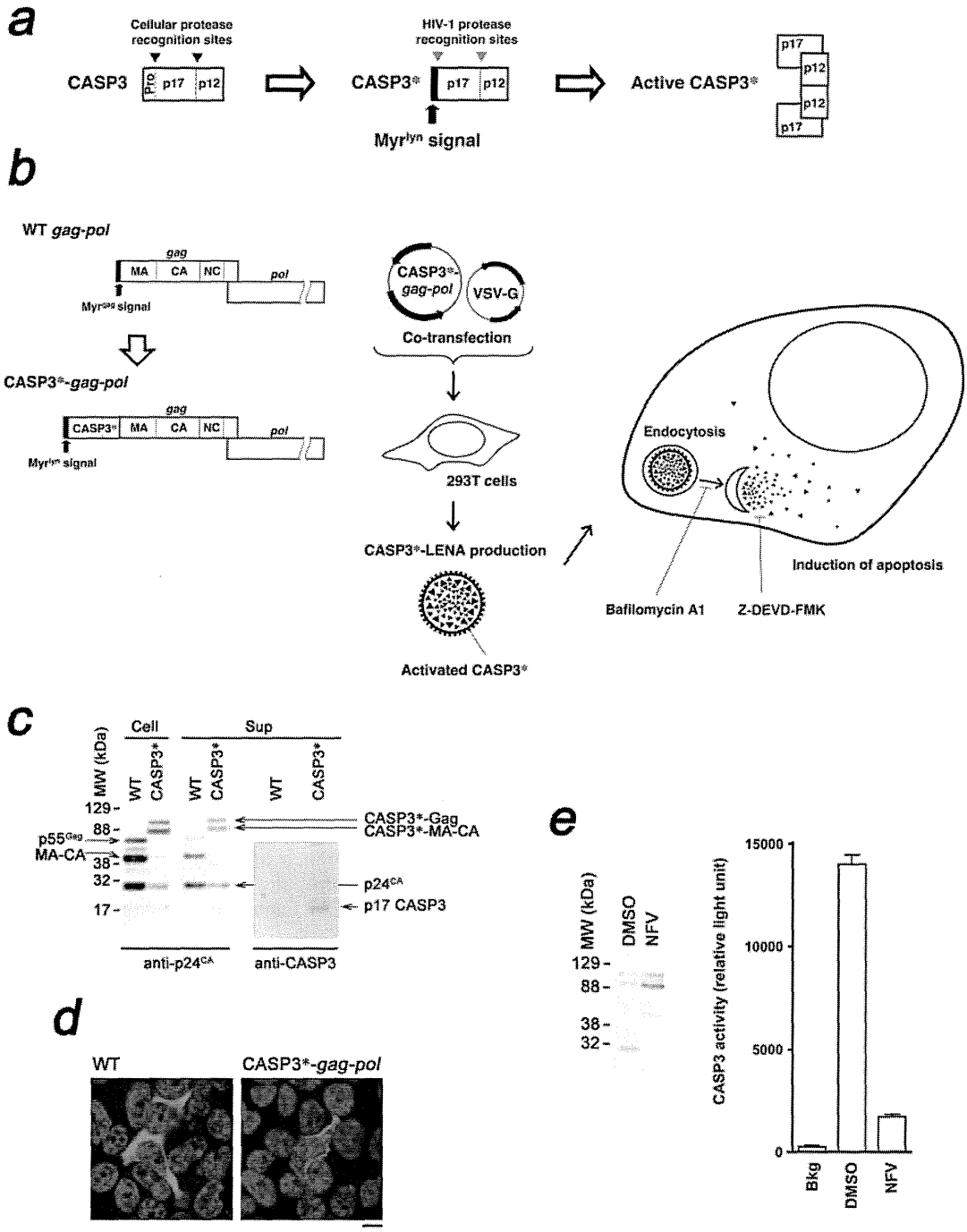

Figure 1 | Construction, production and characterization of CASP3*-LENA. (a) Genetic structure of CASP3 and the genetic modification to produce HIV-1 protease-activable CASP3*. The cellular (gray triangle, digesting D28-S29 and D175-S176 junctions) and HIV-1 (black triangle) protease proteolytic sites are indicated. The CASP3 D28 was replaced with amino acids 127–136 (VSQNYPIVQ) from HIV-1 Gag (according to the HXB2 coordinate). The amino acids 129–134 (QNYPIV) from HIV-1 Gag according to the HXB2 coordinate was inserted after CASP3 D175. HIV-1 protease targets the YP junction. The enzyme is active when the p17 and p12 subunits are dimerized. (b) Production of CASP3*-LENA and its mechanism of action. The *CASP3** was placed at the 5' end of wild type (WT) *gag-pol* to yield CASP3**-gag-pol*. The proteolytic cleavage sites within Gag for HIV-1 protease and the proteolytic products are indicated MA, matrix; CA, capsid; and NC, nucleocapsid. The CASP3**-gag-pol* and VSV-G expression vectors were co-transfected into 293T cells. Then, the VSV-G-encapsidated LENA containing activated CASP3* protein was produced in the culture supernatant. CASP3*-LENA enters cells via an endocytotic route, with the content released from endosomes at the site of membrane fusion. The action points of Bafilomycin A1 (BAF) and the CASP3 inhibitor Z-DEVD-FMK are indicated. (c) Expression of CASP3*-gag-pol and CASP3*-LENA production. The cell lysates (Cell) and culture supernatants (Sup) of 293T cells transfected with either wild type (WT) or CASP3*-gag-pol (CASP3*) expression vector were analyzed by Western Blot. The corresponding protein for each band is indicated. (d) Immunofluorescence assay showing the distribution of WT Gag or CASP3*-Gag (CASP3*) in 293T cells transfected with either WT or CASP3**-gag-pol* (CASP3*) expression vector. Red and blue represent the anti-$p24^{CA}$ monoclonal antibody-stained signal and the Hoechst 33258-stained nucleus, respectively. Magnification, x630; scale bar, 10 μm. (e) Detection of CASP3 enzyme activity in purified CASP3*-LENA. CASP3*-LENA was produced either in the presence or absence of nelfinavir (NFV) and collected by ultracentrifugation over a 20% sucrose layer. DMSO was used as a control. The amount of CASP3*-LENA and the cleavage pattern of Gag were examined by Western blot (left). CASP3 enzyme activity was detected in the CASP3*-LENA lysate (right).

293T cell lysate transfected with pCASP3*-*gag-pol* by Western blot analysis (Fig. 1c, Cell) in a pattern similar to that of wild-type Gag-pol (WT, Fig. 1c). However the processing efficiency of Gag was slightly attenuated in the CASP3* construct compared with WT, as highlighted by the smaller amount of $p24^{CA}$ relative to its precursor. In the culture supernatant of transfected 293T cells, CASP3*-LENA was detected by Western blot analysis (Fig. 1c, Sup). The presence of CASP* was verified by Western blot analysis using anti-CASP3 antibody that specifically recognizes the p17 subunit of CASP3 (Fig. 1c, Sup). In 293T cells transiently transfected with the WT expression plasmid, Gag was evenly distributed in the cell cytoplasm as visualized by an immunofluorescence assay (Fig. 1d). In contrast, CASP3*-Gag was distributed mainly in the cytoplasm and, to a lesser extent, in the nucleus, forming numerous fine aggregations (Fig. 1d). Also, some CASP3*-Gag signal was detected at the cell periphery (Fig. 1d). Despite these differences, LENA production by CASP3*-Gag-pol was as efficient as that by WT; the signal ratio of CASP3*-Gag and its proteolytic products in the virus-like particle (VLP) fraction relative to the cell lysate were comparable to that of the WT (Fig.1c).

To verify the enzyme activity of CASP3* in LENA, the proteolytic activity of CASP3* was measured using a caspase 3/7-specific substrate, DEVD-aminoluciferin, that luminesces upon cleavage. Significant enzymatic activity was detected in the purified CASP3*-LENA (Fig. 1e). Importantly, this signal was substantially reduced when proteolytic cleavage of CASP3*-Gag was attenuated through the preparation of CASP3*-LENA in the presence of 0.5 μM HIV-1 protease inhibitor nelfinavir (NFV; Fig. 1e). These data suggest that active CASP3* is enveloped in the LENA and that the activation of CASP3* is dependent on HIV-1 protease.

HIV-1 protease is fully activated after viral budding. Thus, the majority of CASP3* should be activated outside cells. This minimizes damage to LENA-producing cells by CASP3*. However, LENA-producing 293T cells were damaged upon Gag-pol expression presumably due to the cytotoxicity of the small amount of HIV-1 protease activated in the cell cytoplasm upon overexpression of the protein. Cell viability and LENA production improved when the LENA-producing cells were treated with a low dose of HIV-1 protease inhibitor. Preparation of LENA in the presence of 0.2 μM saquinavir (SQV) increased the LENA yield by approximately 4-fold (Fig. 2a). Under these conditions, HIV-1 protease in LENA remained active as evidenced by the production of cleavage intermediates of CASP3*-Gag (Fig. 2a). The activation of CASP3* was not blocked under these conditions because a cleavage intermediate, MA-CA, predicated the release of CASP3* from the precursor (Fig. 2a, arrowhead), and the biological activity of CASP3*-LENA was detected as described below. Similar data were obtained using the low dose of NFV.

For leukemic cell killing by CASP3*-LENA, an acute T cell lymphoblastic leukemia (ALL) cell line, MOLT-4, was chosen. MOLT-4 cell viability was significantly attenuated when cells were exposed to CASP3*-LENA, whereas no cell killing was observed in WT-LENA or non-enveloped CASP3*-LENA at 1d post-LENA exposure (Fig. 2b and 2c). A cell metabolism-based cell viability assay revealed that 93.3% of cell viability was lost in CASP3*-LENA-exposed MOLT-4 cells at 1d post-LENA exposure (Fig. 2b). This cell killing was more efficient when cells were treated with CASP3*-LENA prepared in the presence of 0.2 μM SQV bearing a higher LENA titer (99.2%, Fig. 2b). The MOLT-4 cells exposed to CASP3*-LENA contained fragmented nuclei with condensed chromatin, characteristic of cells undergoing apoptosis (Fig. 2d). Such nuclear morphology was not found in MOLT-4 cells exposed to WT-LENA or non-enveloped CASP3*-LENA. Induction of apoptotic cell death was detected at 6 h post-LENA exposure by Annexin V staining (Fig. 2e). The VSV-G functional inhibitor Bafilomycin A1, which prevents the endosome acidification required for the activation of VSV-G, rescued the cells from apoptotic cell death at 12.5 ng ml^{-1} (Fig. 2c-f). A cell-permeable CASP3 inhibitor, Z-DEVD-FMK, also protected cells from CASP3*-LENA-induced apoptosis at 0.5 μM (Fig. 2c–g). These data suggest that the cell death induced by CASP3*-LENA is dependent on VSV-G function and the proteolytic function of CASP3*. The death inducing titer of CASP3*-LENA for MOLT-4 cell was 2.0×10^6 particles per milliliter, which was estimated from the dose-dependent cell killing kinetics using serially diluted CASP3*-LENA preparations (average of four independent experiments).

In addition to MOLT-4 cells, CASP3*-LENA induced apoptosis in two more leukemic cell models, SUP-T1 cells, a pleural effusion T cell lymphoblastic lymphoma cell line, and the HTLV-1-transformed T cell line M8166, a model for adult T cell leukemia (ATL, Fig. 2g). Similar data were obtained in the human chronic myelogenous leukemia (CML)-derived cell line K562 and the neuroblastoma cell line NP-2 (data not shown). These data indicate that the cell killing activity of CASP3*-LENA is not restricted to the leukemic cells. In these experiments, WT-LENA and non-enveloped CASP3*-LENA failed to induce apoptosis. These data demonstrate the attractiveness of CASP3* protein transduction by LENA as a tool for molecular cancer therapy. The cell killing activity of CASP3*-LENA was not detected in primary blood mononuclear cells (data not shown). This is presumably because the primary cells are inefficient to the LENA-mediated protein delivery and/or to the CASP3-induced apoptosis, or both. This suggests that the CASP3*-LENA may favor cancer cells to induce apoptotic cell death.

CASP3* was also applied to limit HIV-1 replication. We hypothesized that CASP3*-expressing T cells may be more susceptible to apoptosis upon HIV-1 infection due to the expression of HIV-1 protease in infected cells. To this end, SUP-T1 cells were transduced with CASP3* using a murine leukemia virus (MLV) vector, and two independently isolated pairs of SUP-T1 cells were analyzed (Fig. 3a). The rate of cell proliferation and the susceptibility to apoptosis induced by a serim depriviation in SUP-T1/CASP3* cells were indistinguishable from those in SUP-T1/Cont cells (data not shown). Cells were exposed to a low- or high-dose HIV-1 preparation and viral replication was monitored. In both isolates, HIV-1 propagation in SUP-T1/CASP3* cells was attenuated regardless of the HIV-1 exposure dose (Fig. 3b). These data suggest that CASP3* can limit the propagation of HIV-1 in tissue culture.

To determine the mechanism by which HIV-1 replication is blocked, the viral entry phase and the production phase were investigated separately. If the virus-associated protease is responsible for the activation of CASP3* at the viral entry phase, infection with the HIV-1-based lentiviral vector should also kill SUP-T1/CASP3* cells. Thus, the establishment efficiency of lentiviral vector infection in SUP-T1/CASP3* cells should be lower than that in control cells. To test this, SUP-T1/CASP3* cells were infected with a lentiviral vector expressing luciferase upon establishment of infection. The luciferase activity in SUP-T1/CASP3* cells at 4 d post-infection was lower than in the control cells (Fig. 3c). On the other hand, the levels of MLV-transduced luciferase activity in SUP-T1/CASP3* cells were similar to those in the control cells (Fig. 3c). Note that CASP3* was not activated by MLV since the substrate preference of MLV protease is distinct from that of HIV-1 protease. These data suggest that virus-associated HIV-1 protease is capable of activating CASP3* to induce apoptosis in SUP-T1/CASP3* cells. Luciferase activity was still detected in the lentiviral vector-infected SUP-T1/CASP3* cells (Fig. 3c), implying that some cells might have lost the high-level expression of CASP3* or a single virion-associated protease might not be able to initiate CASP3* activation at levels sufficient to kill all of the infected cells. Next, the induction of apoptosis by the virion-associated viral protease was examined directly. SUP-T1/CASP3* cells were exposed to HIV-1 and the cells were probed with Annexin V. At 6 h post-infection, 2.7% of SUP-T1/

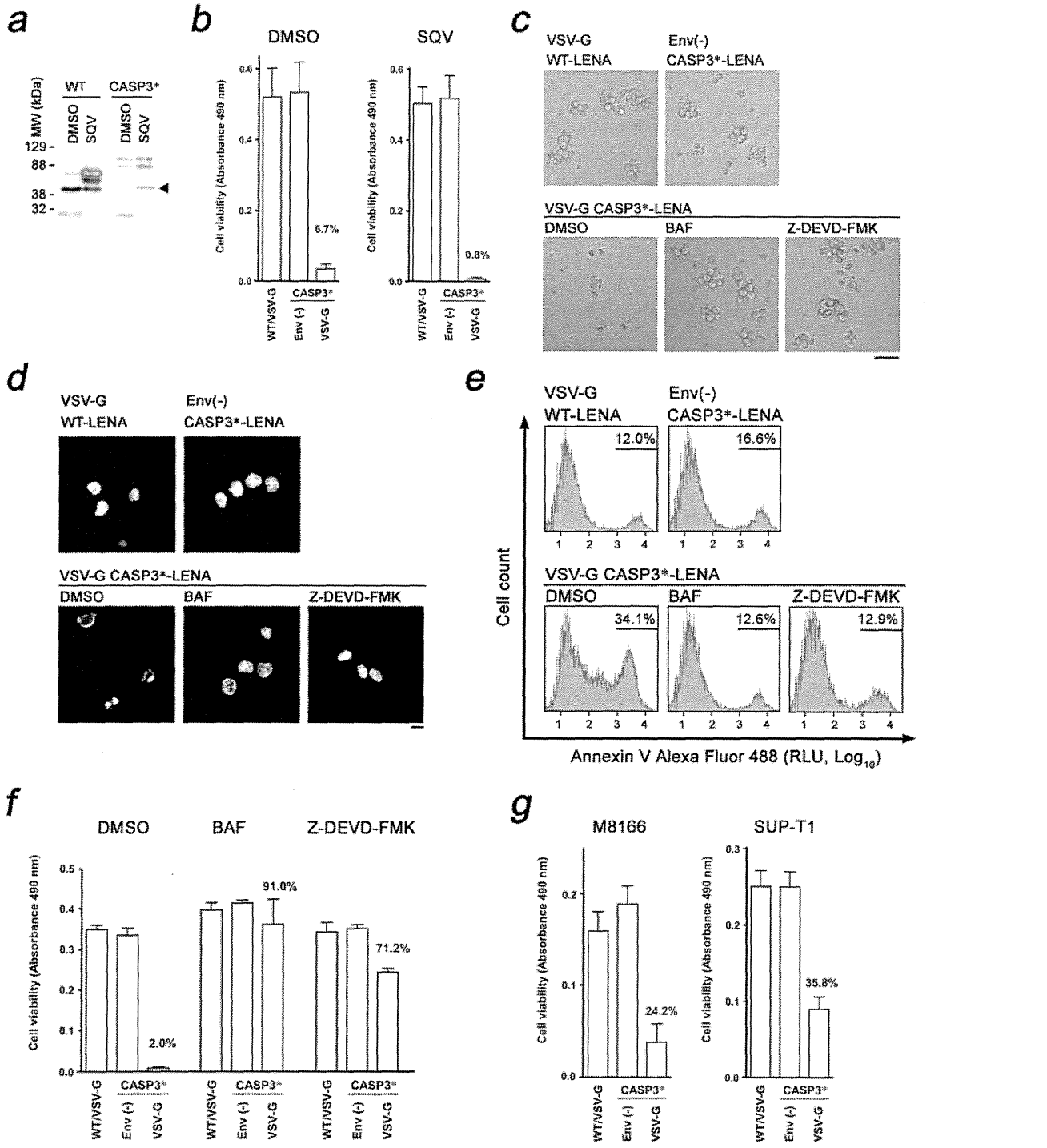

Figure 2 | Induction of apoptosis in leukemic cells by CASP3*-LENA. (a) Enhancement of WT- and CASP3*-LENA production by a low dose of saquinavir (SQV, 0.2 μM). DMSO was used as a solvent control. The arrowhead indicates a signal representing the MA-CA, indicating the release of CASP3* from CASP3*-Gag. (b) Quantitative analysis of MOLT-4 cell viability after LENA exposure. Cell viability was scored by colorimetric assay at 1d post-LENA exposure comparing WT-LENA encapsidated with VSV-G (WT/VSV-G), non-enveloped CASP3*-LENA (ENV(-)), and CASP3*-LENA encapsidated with VSV-G. The average and standard deviation from triplicated wells using LENA produced in the presence or absence of SQV are shown (SQV and DMSO, respectively). (c) Light microscopic observation of MOLT-4 cells treated with LENA produced in the presence of low-dose SQV. Cells were imaged at 1 d post-LENA exposure. Cells were treated with either Bafilomycin A1 (BAF) or the CASP3 inhibitor Z-DEVD-FMK. DMSO was used as a solvent control. Bar, 50 μm; magnification x100. (d) Nuclear morphology of MOLT-4 cells treated with LENA produced in the presence of low-dose SQV. Cells were imaged at 1 d post-LENA exposure after staining with Hoechst dye. Cells were treated with either BAF or Z-DEVD-FMK. DMSO was used as a solvent control. Bar, 10 μm; magnification x630. (e) Flow cytometric detection of apoptotic MOLT-4 cells. Cells were stained with Annexin V Alexa Fluor 488 at 6 h post-exposure to LENA produced in the presence of low dose nelfinavir (NFV, 0.2 μM). The live cell fraction was gated to analyze the early phase of apoptotic cell death. Cells were treated with either BAF or Z-DEVD-FMK. DMSO was used as a solvent control. RLU, relative light units. (f) Quantitative analysis of MOLT-4 cell viability after exposure to LENA produced in the presence of low-dose NFV (0.2 μM). Cell viability was scored at 1d post-LENA exposure. Cells were treated with either BAF or Z-DEVD-FMK. DMSO was used as a solvent control. (g) Quantitative analysis of M8166 and SUP-T1 cell viabilities as perfomed on MOLT-4 cells.

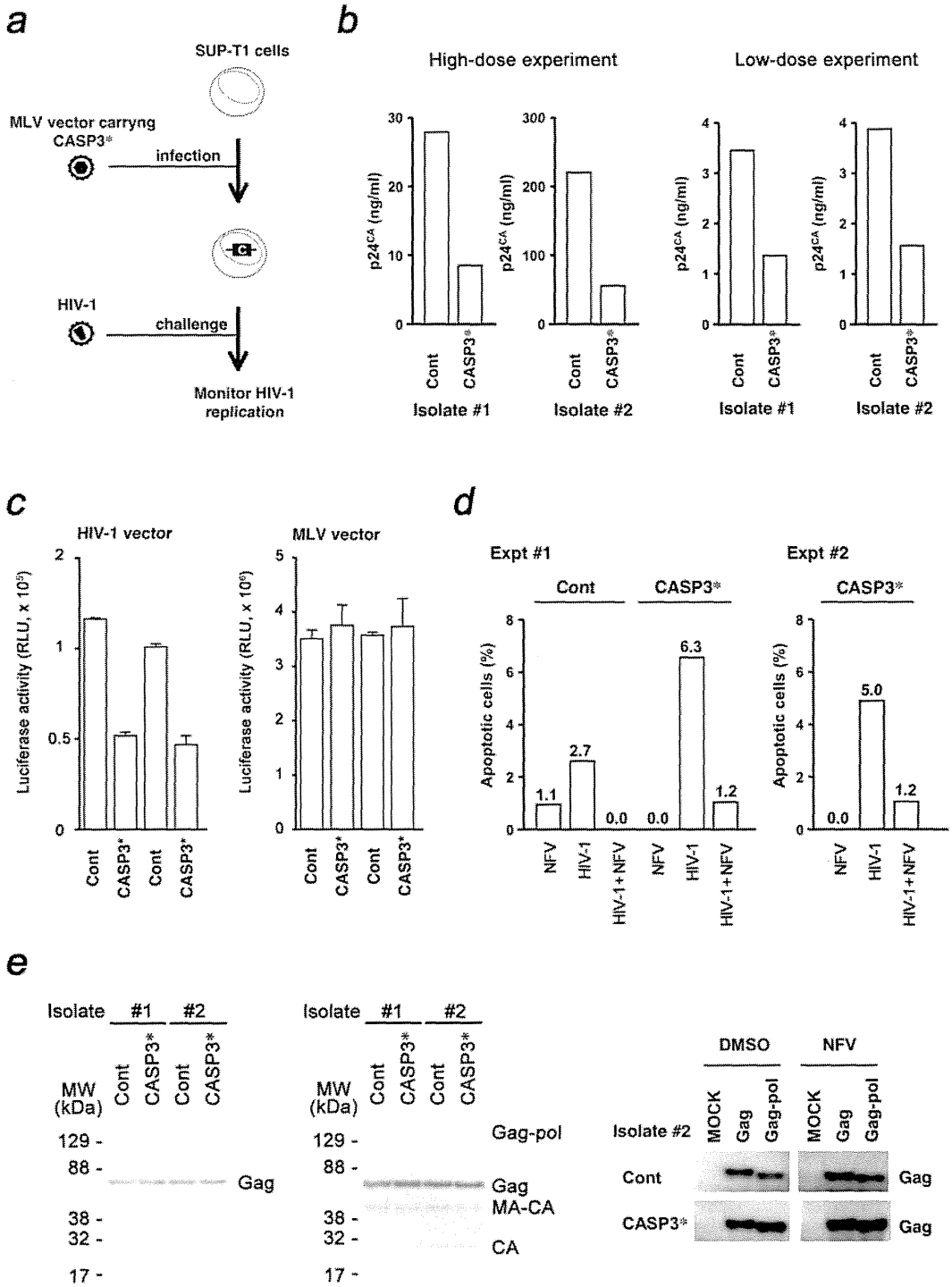

Figure 3 | Inhibition of HIV-1 propagation by CASP3*. (a) Schematic representation of the experimental approach. SUP-T1 cells were infected with MLV carrying the *CASP3** to produce cells constitutively expressing CASP3*. These cells were infected with HIV-1, and the replication efficiency of HIV-1 was measured using viral $p24^{CA}$ antigen in the cell culture medium. (b) Inhibition of $HIV\text{-}1_{NL4\text{-}3}$ replication in SUP-T1/CASP3* cells. Cells were exposed to high- or low-dose viral preparation yielding 25 ng or 1.3 ng of $p24^{CA}$ per 1×10^5 cells, respectively. The viral $p24^{CA}$ concentration in the culture supernatant was measured at 6–9 d post-viral infection. Results shown were obtained from two independent isolates of SUP-T1/CASP3* and control cells. (c) Analysis of SUP-T1/CASP3* cell fate after HIV-1 entry. Luciferase activity of cells infected with either an HIV-1-based lentiviral vector or an MLV vector was measured at 4 d post-infection. RLU, relative light units. (d) Flow cytometric detection of apoptotic SUP-T1/Cont and SUP-T1/CASP3* cells by $HIV\text{-}1_{NL4\text{-}3}$ infection. The percentage of Annexin V Alexa Fluor 488 positive cells was measured at 6 h post-nelfinavir (NFV) exposure, post-HIV-1 infection, and post-HIV-1 infection in the presence of 2 μM NFV, and subtracted from the percentage of Annexin V positive cells in untreated controls. The live cell fraction was gated according to scatter to analyze the early phase of apoptotic cell death. Data from two independent experiments are shown. For this experiment, cells from isolate #2 were used. (e) Analysis of SUP-T1/CASP3* cell fate upon HIV-1 production. The SUP-T1/CASP3* cells were transduced with HIV-1 Gag-pol or Gag by either MLV vector (left panel) or transfection (right panel), and the expression of transduced proteins was detected at 7 d post-gene transduction by Western blot. For the transfection experiment, cells were maintained in the presence of 0.5 μM NFV to detect the effect of Pol on cell survival.

Cont cells underwent apoptosis, which was lowered by NFV (Fig. 3d), suggesting that the HIV-1 infection induces apoptotic cell death in a HIV-1 protease-dependent manner as previously reported[9,10]. By contrast, the apoptotic cells was detected more frequently in SUP-T1/CASP3* cells than in SUP-T1/Cont cells (6.3% and 5.0% in two independent experiments), which was drastically decreased to 1.2% in the presence of NFV (Fig. 3d). These data suggest that the CASP3* predispose cells to undergo apoptosis upon HIV-1 infection, and the virus-associated protease is responsible for the induction of apoptosis.

To examine the viral production phase, the HIV-1 *gag-pol* was transduced into SUP-T1/CASP3* cells by MLV vector, and the levels of Gag were evaluated. If HIV-1 protease activity in virus producing cells is responsible for the activation of CASP3*, then the expression of Gag-pol, not Gag, should confer the cell growth disadvantage, resulting in reduced levels of Gag in these cells. Transfected SUP-T1/CASP3* cells were subjected to Western Blot analysis at 7 d post-infection. The levels of Gag and its proteolytic products in SUP-T1/CASP3* cells were indistinguishable from those of the control cells (Fig. 3e). Similar results were obtained when SUP-T1/CASP3* cells were transfected with a plasmid expressing HIV-1 Gag-pol (Fig. 3e). These data indicate that the attenuation of HIV-1 replication in SUP-T1/CASP3* cells is due to the activation of CASP3* by virion-associated HIV-1 protease at the viral entry phase, leading to the depletion of virus-infected cells from the culture by apoptosis. In agreement with this model, the inhibition of apoptosis by Z-DEVD-FMK enhanced the efficiency of HIV-1 replication (data not shown).

Discussion

This study provides evidence that CASP3* has therapeutic potential against cancer and HIV-1 infection, overcoming the potential difficulty of CASP3 for the application to human gene therapy[3,4,11]. The cancer therapy by CASP3*-LENA may be more applicable to solid tumors due to the current technological limit in particle delivery. However, to apply the CASP3*-LENA approach to the cancer therapy, it is critical to improve the potency of CASP3*-LENA. This is because the cell killing activities of CASP3*-LENA in some transformed cells, including MT-4, a HTLV-1-transformed human T cell line, were undetectable although the LENA-mediated protein delivery by LENA has been shown to be highly efficient in MT-4 cells[6]. MT-4 cells are highly resistant to apoptosis because they express potent anti-apoptotic genes, such as HTLV-1 Tax[12–14]. The Tax induces expression of intracellular caspase inhibitor, cFLIP, which inhibits the activation cycle of CASPs[15,16]. Cancer cells often express high levels of cellular inhibitor of apoptosis protein (CIAP), which may lower the susceptibility of cells to apoptosis induced by CASP3. We may be able to overcome this issue by generating a CASP3* mutant that does not interact with CIAP. The potentiation of CASP3*-LENA should also contribute to reduce the number of injections necessary to achieve the therapeutic effect. Additionally, for clinical applications, a regulatory system to control the cell tropism of LENA needs to be developed.

For HIV-1 infection, CASP3* may be applicable to adoptive stem cell therapy, alternatively termed intracellular vaccination. Stem cell gene therapy has been shown to be effective in clinical trials against HIV-1 infection, as has shRNA therapy targeting CCR5 mRNA[7]. Gene therapy using a zinc finger nuclease was found to be effective against HIV-1 infection as well[8]. These therapeutic approaches target nucleic acids, and off-target effects represent a serious concern. CASP3* is designed to be activated specifically by HIV-1 protease; thus, it offers a basis for a novel therapeutic approach with few "off-target" effects. CASP3* induces suicide in HIV-1-infected cells, and does not yield latently-infected cells. The CASP3* approach should be effective against drug-resistant HIV-1 strains since the anti-viral mechanism of CASP3* is distinct from those of currently-available anti-retroviral drugs. Furthermore, a CASP3*-resistant HIV-1 may not emerge easily. This is because mutations in viral protease that do not affect Gag processing but also do not activate CASP3* are unlikely to occur. Additionally, our strategy is applicable to other infectious diseases if the infectious agents encode proteases with unique substrate preferences. In summary, our work provides a platform for the development of a CASP3*-based therapy against cancer and HIV-1 infection.

Methods

Plasmids. *CASP3* was amplified from MT-4 total RNA using a two-step PCR protocol. For the first reaction, two RT-PCR reactions were performed using the following primer sets: fwd #1 5'-acc ggt cAG CCA GAA CTA Ccc cat cgt gca gTC Tgg aat atc cct gga caa c-3' and rev #1 5'-CTc acg atg ggG TAG TTC TGg tct gtc tca atg cca cag tc-3'; and fwd #2 5'-acC AGA ACT ACc cca tcg tgA GTG GTG TTG ATG ATG ACA TGG-3' and rev #2 5'-CAA TTG GTG ATA AAA ATA GAG TTC TTT TG-3'. The second PCR reaction was performed using fwd #1 and rev #2 primers targeting the products obtained in the first RT-PCR reactions. The *AgeI-MfeI* fragment of the PCR product was cloned into *AgeI-EcoRI* sites of *plynMyGFP-gag-pol*[6], generating pCASP3*-*gag-pol*. The retroviral expression vector pQcCASP3* was constructed by amplifying *CASP3** by PCR as detailed above using 5'-acc ggt gcc acc ATG ggc TCT gga ata tcc ctg gac aac-3' and 5'-CAA TTG TTA GTG ATA AAA ATA GAG TTC TTT TG-3', and cloned into *AgeI-EcoRI* sites of pQcXIP (Clontech, Palo Alto, CA). The pCMMP Gagf vector was constructed by cloning a *XhoI-BamHI* fragment from pGag-GFP[17] into the corresponding restriction sites of pCMMP KRAB[18]. The pCMMP HIV-1 *gag-pol* IRES GFP was constructed by three step cloning. First, the *AgeI-BamHI* KRAB gene fragment from pCMMP KRAB was cloned into the corresponding restriction sites of pCMMP LacZ IRES GFP[9], generating pCMMP KRAB IRES GFP. The *AgeI-EcoRI BlaM* gene fragment amplified from pUC19 by PCR[6] was cloned into the *AgeI-MfeI* sites of pCMMP KRAB IRES GFP, generating pCMMP BlaM IRES GFP. The *EcoRI-XhoI* HIV-1 *gag-pol* gene fragment from p*gag-pol*[18] was cloned into the corresponding restriction sites of pCMMP BlaM IRES GFP, generating pCMMP HIV-1 *gag-pol* IRES GFP. The HIV-1 proviral DNA pNL4-3 was obtained from the NIH AIDS Research and Reference Program. The HIV-1 Gag expression vector pHIV-1 Gagf was produced by cloning an *AgeI-BamHI* fragment from pHIV-1 Gagf-GFP[17] into the corresponding sites of pEGFP-C2 (Clontech).

Cells, viability assay, and transfection. Cells were maintained in RPMI 1640 medium (Sigma, St. Louis, MA) supplemented with 10% fetal bovine serum (Japan Bioserum, Tokyo), 100 U ml^{-1} penicillin, and 100 μg ml^{-1} streptomycin (Invitrogen), at 37°C in a humidified 5% CO_2 atmosphere. Cells were transfected with Lipofectamine 2000 according to the manufacturer's protocol (Invitrogen). Bafilomycin A1 was used at a concentration of 12.5 ng ml^{-1} (Sigma), and a CASP3 inhibitor, Z-DEVD-FMK, was used at a concentration of 0.5 μM (BioVision, Mountain View, CA). The HIV-1 protease inhibitors nelfinavir (NFV) and saquinavir (SQV) were obtained from the NIH AIDS Research and Reference Reagent Program. To produce VSV-G-pseudotyped LENA, 200 ng pVSV-G (Clontech) and 2 μg pCASP3*-gag-pol or *pgag-pol*[18] were transfected into 293T cells. Non-enveloped LENA was produced using pcDNA3 (Invitrogen) in place of pVSV-G. The LENA preparation was passed through nitrocellulose filters (0.45 μm). Cell viability was scored by the CellTiter 96 Aqueous One Solution Cell Proliferation Assay (Promega). For the transfection of plasmids into SUP-T1 cells, a DEAE-dextran protocol was employed. Five million cells were resuspended in 250 μl of STBS (25 mM TrisCl, pH 7.4, 137 mM NaCl, 5 mM KCl, 0.6 mM Na_2HPO_4, 0.7 mM $CaCl_2$, and 0.5 mM $MgCl_2$), including 10 μg of plasmid DNA. Cells were mixed with 250 μl of STBS containing 1 mg ml^{-1} of DEAE-dextran and incubated for 30 min at room temperature (RT). The cells were then incubated with STBS containing 10% DMSO for 2 min at RT and washed with 1 ml HBSS (Invitrogen).

Protein transduction. Protein transduction was performed as described previously by incubating approximately 1×10^6 cells with 1 ml LENA-containing culture medium at 37°C[3].

Immunological detection. The detection of viral gene products by Western blot analysis was performed as described previously[19], except that the anti-$p24^{CA}$ monoclonal antibody clone 183-H12-5C and anti-CASP3 p17 subunit polyclonal antibody (Cat. # AB3623, Millipore, Tokyo, Japan) were used. Immunofluorescent analysis was performed as described previously using the same monoclonal antibody[18]. Signals were detected using an LAS-3000 mini Lumino-Image analyzer operated by the LAS-300mini Image Reader software (ver.2.2, Fuji Film, Tokyo, Japan). The brightness and contrast of the image were adjusted using Adobe Photoshop (ver.7.0, Adobe, Tokyo, Japan).

Microscopy. Cells were imaged by confocal fluorescence microscopy (LSM510 Meta, Carl Zeiss MicroImaging Inc., Tokyo, Japan). For the imaging of nuclei, multiple focal planes were projected to generate a single image.

Virus production and infection. The HIV-1, lentiviral and MLV vectors used have been described previously[9]. The pQcXIP was used as a control for pQcCASP3*.

Detection of CASP3 enzymatic activity. The substrate for the CASP3 enzyme assay was purchased from Promega (Caspase-Glo 3/7 Assay System, Promega, Madison, WI). Luciferase activity was measured using the Steady-Glo Luciferase Assay system (Promega). Luminescence was detected using a Veritas™ Microplate Luminometer (Promega).

Annexin V apoptosis assay. Cells were analyzed by flow cytometry using the Vybrant Apoptosis Assay kit (Invitrogen).

Enzyme-Linked Immunosorbent Assay (ELISA). A p24 ELISA was conducted according to the manufacturer's protocol (Zeptometrics, Buffalo, NY). To measure cellular p24, transfected 293T cells were washed once with PBS, lysed in 500 μl buffer A (described above) for 30 min, and then subjected to the ELISA.

1. Cohen, G. M. Caspases: the executioners of apoptosis. *Biochem J.* **326**, 1–16 (1997).
2. Boatright, K. M. & Salvesen, G. S. Mechanisms of caspase activation. *Curr Opin Cell Biol.* **15**, 725–31 (2003).
3. Yamabe, K. *et al.* Cancer gene therapy using a pro-apoptotic gene, caspase-3. *Gene Ther.* **6**, 1952–9 (1999).
4. Cam, L., Boucquey, A., Coulomb-L'hermine, A., Weber, A. & Horellou, P. Gene transfer of constitutively active caspase-3 induces apoptosis in a human hepatoma cell line. *J Gene Med.* **7**, 30–8 (2005).
5. Walters, J. *et al.* A constitutively active and uninhibitable caspase-3 zymogen efficiently induces apoptosis. *Biochem J.* **424**, 335–45 (2009).
6. Aoki, T., Miyauchi, K., Urano, E., Ichikawa, R. & Komano, J. Protein transduction by pseudotyped lentivirus-like nanoparticles. *Gene Ther* **18**, 936–941 (2011).
7. Mitsuyasu, R. T. *et al.* Phase 2 gene therapy trial of an anti-HIV ribozyme in autologous CD34+ cells. *Nat Med.* **15**, 285–92. Epub 2009 Feb 15. (2009).
8. Holt, N. *et al.* Human hematopoietic stem/progenitor cells modified by zinc-finger nucleases targeted to CCR5 control HIV-1 in vivo. *Nat* **28**, 839–47 (2010).
9. Komano, J., Miyauchi, K., Matsuda, Z. & Yamamoto, N. Inhibiting the Arp2/3 complex limits infection of both intracellular mature vaccinia virus and primate lentiviruses. *Mol Biol Cell.* **15**, 5197–207. Epub 2004 Sep 22. (2004).
10. Nicholson, D. W. *et al.* Identification and inhibition of the ICE/CED-3 protease necessary for mammalian apoptosis. *Nature.* **376**, 37–43 (1995).
11. Wagner, R. *et al.* Rev-independent expression of synthetic gag-pol genes of human immunodeficiency virus type 1 and simian immunodeficiency virus: implications for the safety of lentiviral vectors. *Hum Gene Ther* **11**, 2403–13 (2000).
12. Shaulian, E. & Karin, M. AP-1 as a regulator of cell life and death. *Nat Cell Biol.* **4**, E131-6 (2002).
13. Azran, I., Schavinsky-Khrapunsky, Y. & Aboud, M. Role of Tax protein in human T-cell leukemia virus type-I leukemogenicity. *Retrovirology.* **1**, 20 (2004).
14. Charoenthongtrakul, S., Zhou, Q., Shembade, N., Harhaj, N. S. & Harhaj, E. W. Human T cell leukemia virus type 1 Tax inhibits innate antiviral signaling via NF-kappaB-dependent induction of SOCS1. *J Virol.* **85**, 6955–62. Epub 2011 May 18. (2011).
15. Krueger, A. *et al.* HTLV-1 Tax protects against CD95-mediated apoptosis by induction of the cellular FLICE-inhibitory protein (c-FLIP). *Blood.* **107**, 3933–9. Epub 2006 Jan 10 (2006).
16. Okamoto, K., Fujisawa, J., Reth, M. & Yonehara, S. Human T-cell leukemia virus type-I oncoprotein Tax inhibits Fas-mediated apoptosis by inducing cellular FLIP through activation of NF-kappaB. *Genes Cells.* **11**, 177–91 (2006).
17. Aoki, T. *et al.* Improvement of lentiviral vector-mediated gene transduction by genetic engineering of the structural protein Pr55 Gag. *Gene Ther* **17**, 1124–33 (2010).
18. Urano, E. *et al.* Substitution of the myristoylation signal of human immunodeficiency virus type 1 Pr55Gag with the phospholipase C-delta1 pleckstrin homology domain results in infectious pseudovirion production. *J Gen Virol.* **89**, 3144–9 (2008).
19. Shimizu, S. *et al.* Inhibiting lentiviral replication by HEXIM1, a cellular negative regulator of the CDK9/cyclin T complex. *Aids.* **21**, 575–82 (2007).

Acknowledgments

This work was supported by the Japan Health Science Foundation, the Japanese Ministry of Health, Labor, and Welfare (H18-AIDS-W-003 to JK), and the Japanese Ministry of Education, Culture, Sports, Science and Technology (18689014 and 18659136 to JK).

Author contributions

K.M., E.U., M.T., R.I., and J.K. designed and performed experiments and interpret the data. J.K. wrote the manuscript. K.M. and E.U. equally contributed to this work.

Additional information

Competing financial interests: The authors declare no competing financial interests.

How to cite this article: Miyauchi, K., Urano, E., Takizawa, M., Ichikawa, R. & Komano, J. Therapeutic potential of HIV protease-activable CASP3. *Sci. Rep.* **2**, 359; DOI:10.1038/srep00359 (2012).

Gene 505 (2012) 1–8

Contents lists available at SciVerse ScienceDirect

Gene

journal homepage: www.elsevier.com/locate/gene

Regulation of cyclin T1 expression and function by an alternative splice variant that skips exon 7 and contains a premature termination codon

Emiko Urano, Kosuke Miyauchi [1], Reiko Ichikawa, Yuko Futahashi, Jun Komano *

AIDS Research Center, National Institute of Infectious Diseases, 1-23-1 Toyama, Shinjuku-ku, Tokyo 162-8640, Japan

ARTICLE INFO

Article history:
Accepted 4 June 2012
Available online 9 June 2012

Keywords:
Cyclin T1 (CCNT1)
Alternative splicing
Exon skipping
Premature termination codon (PTC)
Nonsense-mediated mRNA decay (NMD)
Human immunodeficiency virus type 1 (HIV-1)

ABSTRACT

Cyclin T1 (*CCNT1*), a gene containing nine exons, forms the positive transcription elongation factor b (P-TEFb) complex and regulates a wide variety of biological processes including transcription. We discovered a novel splice variant of *CCNT1* that lacks exon 7 (*dE7*). RT-PCR analysis revealed that the dE7 transcript was detected in almost all tissues examined. The dE7/FL transcript ratio was high in quiescent peripheral blood mononuclear cells (PBMC) and in tissues poor in cell division; however, it was low in activated PBMC and in tissues with high cell proliferative potential. These results suggest that exon 7 skipping is linked to cell cycle progression. Increasing the *dE7/FL* transcript ratio resulted in the reduction of CCNT1 protein levels, indicating that the expression of CCNT1 protein is controlled by exon skipping. Exon 7 skipping yields a +1 frameshift at exon 8, which generates a premature termination codon (PTC). The *dE7* transcript levels increased when cells were treated with the protein synthesis inhibitor cycloheximide (CHX) or a kinase inhibitor wortmannin (WORT), whilst the *FL* transcript levels were unchanged, suggesting that the *dE7* transcript is a target of nonsense-mediated decay (NMD). Importantly, reduction of *dE7* transcript by WORT correlated well with the decrement of CCNT1 protein expression. The *dE7* transcript would produce an approximately 23 kDa protein that covers approximately 70% of the cyclin box. The ectopically expressed dE7 protein physically interacted with CDK9 and competed with FL CCNT1 for CDK9, thus should act dominant-negatively on FL CCNT1. The replication of human immunodeficiency virus type 1 (HIV-1), heavily dependent on the CCNT1 function, was inhibited by dE7 protein through the attenuation of Tat/long terminal repeat (LTR)-driven transcription. Taken together, these results suggest that *dE7* is a novel splice variant that regulates the expression and function of *CCNT1*.

1. Introduction

Transcription is a highly regulated process that responds to many physiological stimuli. The positive transcription elongation factor b (P-TEFb) complex, which consists of cyclin T1/T2 and CDK9, is one of the key regulators of transcription and elongation by RNA polymerase II (RNAP II) (Bres et al., 2008; Garriga and Grana, 2004; Marshall and Grana, 2006; Peterlin and Price, 2006; Zhou and Yik, 2006). Cyclin T1 (CCNT1) is the major component of the P-TEFb complex. The P-TEFb complex phosphorylates the C-terminal domain of RNAP II that drives transcriptional elongation. The P-TEFb complex is involved in differentiation of neurons (De Falco et al., 2005), muscle cells (De Falco and De Luca, 2006), megakaryocytes (Elagib et al., 2008), and lymphocytes (De Falco et al., 2008; Leucci et al., 2007). Recent reports suggest that the P-TEFb complex is also involved in alternative splicing (Barboric et al., 2009), mRNA transport (Rechter et al., 2009), and chromatin modification (Pirngruber et al., 2009).

The P-TEFb complex is bound by many cellular factors, suggesting that the function of this complex is tightly regulated (Bres et al., 2009; Nguyen et al., 2001; Yang et al., 2001, 2008; Zhou and Yik, 2006). Transcription of the long terminal repeat (LTR) of the human immunodeficiency virus (HIV) promoter strongly depends on the P-TEFb complex (Wei et al., 1998; Zhou and Yik, 2006). In fact, CCNT1 was originally identified as a cellular protein that supports the function of Tat, a viral enhancer of LTR transcription (Wei et al., 1998).

Unlike other cyclins, transcriptional-type cyclins are expressed throughout the cell cycle. *CCNT1* expression is increased on cell activation (Herrmann et al., 1998). In most cell types, upregulation of *CCNT1* expression occurs at the transcriptional level (Garriga et al., 1998; Herrmann et al., 1998). By contrast, the expression of *CCNT1* is regulated post-transcriptionally in primary monocytes and macrophages (Herrmann et al., 1998; Liou et al., 2002, 2006; Sung and Rice,

Abbreviations: P-TEFb, positive transcription elongation factor b; PBMC, peripheral blood mononuclear cells; CHX, cycloheximide; WORT, wortmannin; HIV, human immunodeficiency virus; LTR, long terminal repeat; AMA, α-amanitin; PHA, phytohemagglutinin.

* Corresponding author at: Osaka Prefectural Institute of Public Health, Department of Infectious Diseases, Virology Division, 3-69, Nakamachi, 1-chome, Higashinari-ku, Osaka 537-0025, Japan. Fax: +81 3 5285 5037.
E-mail address: ajkomano@nih.go.jp (J. Komano).
[1] Current address: Research Center for Allergy and Immunology, RIKEN Yokohama Institute, 1-7-22 Suehiro-cho, Tsurumi, Yokohama, Kanagawa 230-0045, Japan.

0378-1119/$ – see front matter © 2012 Elsevier B.V. All rights reserved.
doi:10.1016/j.gene.2012.06.006

2006, 2009). $CD4^+$ T cells, monocytes, and macrophages are known to express *CCNT1* at low levels (Herrmann et al., 1998; Liou et al., 2002, 2006; Sung and Rice, 2006). It is hypothesized that the low levels of *CCNT1* in these cells partly accounts for their poor susceptibility to HIV-1 replication (Garriga et al., 1998; Herrmann et al., 1998; Sung and Rice, 2006). The stability of mRNA has been also implicated in the regulation of CCNT1 expression (Marshall et al., 2005). The molecular regulation of *CCNT1* expression, both at the transcriptional and post-transcriptional levels, has been largely unclear.

CCNT1 has nine exons and encodes an 87 kDa protein. CCNT1 is expressed from an ~8 kb mRNA (Wei et al., 1998). Three tissue-specific splice variants have been described: an ~9.5 kb mRNA specifically expressed in primary blood lymphocytes (PBL), an ~3.5 kb mRNA expressed in ovary, and an ~3.0 kb mRNA expressed in testis (Wei et al., 1998). The physiological significance of tissue-specific splice variants has not been characterized. No *CCNT1* splice variant has been documented that is expressed in a wide variety of cell types.

We examined a genetic link between disease progression of HIV-1 infection and cellular HIV-1 regulatory genes. Through this study, we discovered a novel splice variant of *CCNT1* that lacks exon 7 (*dE7*). The *dE7* variant is expressed in diverse tissues and is more abundant than the full length (*FL*) transcript. In this study, we characterized the physiological role of the *dE7* transcript in the regulation of *CCNT1* function.

2. Materials and methods

2.1. RT-PCR

The 5′ half of *Cyclin T1* was amplified by RT-PCR using the following primers: 5′-CAC CGC CAC CAT GGA GGG AGA GAG GAA GAA CAA CAA C-3′ (1F) and 5′-GCT AAA TTC TCA CTA GTC CGA TGA CCC-3′ (9-1R). The 3′ half of cyclin T1 was amplified by RT-PCR using the following primers: 5′- GGG TCA TCG GAC TAG TGA GAA TTT AGC-3′ (9F) and 5′- CCC GGG CCT CGA GCT CTT AGG AAG GGG TGG AAG TGG TGG -3′ (9-EndR). The expected RT-PCR product for the CCNT1 FL transcript is 1077 bp, whereas the *dE7* transcript is 913 bp. The region from exon 6 to the beginning of exon 9 was amplified by RT-PCR using the following primers: 5′-CAA GCA AGG ACT TAG CAC AGA C-3′ (6F) and 5′-CAA CAT CTC CAC ACT GGT TAA GTT GC-3′ (9-2R). The expected RT-PCR product for the *CCNT1 FL* transcript is 491 bp, whereas the *dE7* transcript is 327 bp. The RT-PCR primers for c-myc were 5′-CAG CGA CTC TGA GGA GGA AC-3′ and 5′-CTT GAC CCT CTT GGC AGC AG-3′. The RT-PCR products were separated by either agarose gel or polyacrylamide gel electrophoresis, and visualized by ethidium bromide or sybergreen, respectively. The PCR products were imaged by Typhoon9400 and analyzed by ImageQuant software (GE Healthcare) or ImageJ software (ver 1.45 s, http://imagej.nih.gov/ij). The cDNA panel MTC was purchased from Clontech (Human Blood Fractions MTC Panel and Human MTC Panel I, Clontech, Palo Alto, CA). The cells were activated with the following conditions in the Human Blood Fractions MTC Panel: peripheral blood mononuclear cells (PBMC) by 2 μg/ml pokeweed mitogen (PWM) and 5 μg/ml concanavalin A (Con A) for 3 days, $CD19^+$ cells by 2 μg/ml PWM for 4 days, $CD4^+$ cells by 5 μg/ml Con A for 3–4 days, and $CD8^+$ cells by 5 μg/ml phytohemagglutinin (PHA) for 3 days.

2.2. Cells and transfection

Cells were maintained in RPMI 1640 medium (Sigma, St. Louis, MO) supplemented with 10% fetal bovine serum (Japan Bioserum, Tokyo), 100 U/ml penicillin, and 100 μg/ml streptomycin (Invitrogen, Tokyo, Japan). Cells were then incubated at 37 °C in a humidified 5% CO_2 atmosphere. PBMC were isolated by Ficoll–Conray density centrifugation from healthy donors. PBMC were activated by PHA (Wako, Tokyo, Japan), or a combination of anti-CD3 monoclonal antibody (OKT3, Janssen Pharmaceutical) and recombinant human IL-2 (Shionogi Pharmaceutical). Cycloheximide (CHX) was purchased from Sigma. Wortmannin (WORT) was purchased from Cell Signaling Technology (Danvers, MA). Cells were transfected with Lipofectamine 2000 according to the manufacturer's protocol (Invitrogen). NP2CD4CCR5 cells were generous gift from Dr. Kusagawa (National Institute of Infectious Diseases, Tokyo, Japan).

2.3. Plasmids

The expression plasmids for untagged CCNT1 and FLAG-tagged beta-glucuronidase (GUS), pMAT CCNT1 and pMAT fGUS, were generous gifts from Dr. Fukazawa (NIID, Japan). The expression plasmid for FLAG-tagged CCNT1, pGFP-CCNT1, pMAT fCCNT1, and hemagglutinin (HA)-tagged CDK9 was described previously (Urano et al., 2008). The following plasmids were described previously: pLTR-luc, pSVtat, pHXB2, pCMMP eGFP and pCMMP KRAB IRES GFP (Komano et al., 2004). pCMMP GFPf was described previously (Urano et al., 2010). pJR-CSF was a generous gift from Dr. Koyanagi (Kyoto University, Japan). The FLAG-tagged dE7 cDNA was amplified from CEM cellular RNA by RT-PCR using the following primers: 5′-CAC CGT CGA CCA CCA TGG ACT ACA AAG ACG ATG ACG ACG AGG GAG AGA GGA AGA ACA ACA ACA AAC G-3′ and 5′-CCC GGG TGT GTC AGT TCT GTT GGT TGC CAT G-3′. The RT-PCR product was cloned into the pcDNA6.2/V5/GW/D-TOPO (Invitrogen), and the Xho I–Xma I fragment from the cloned dE7 gene fragment was cloned into the Xho I–Age I site of pEGFP-N1 (Clontech), generating the fdE7-GFP expression vector pfCCNT1dE7-GFP. pMAT fdE7-GFP was constructed by cloning the SnaB I–Hpa I fragment from pfCCNT1dE7-GFP into the SnaB I–Hpa I site of pMAT fCCNT1. The following oligonucleotides 5′-CCG GTC AAT TGT CGC GAG CGG CCG CG-3′ and 5′-GAT CCG CGG CCG CTC GCG ACA ATT GA-3′ were annealed and ligated into the Age I–Bam HI site of pCMMP eGFP to generate pCMMP AMNNB. pCMMP fdE7-GFP was constructed by cloning blunted Age I-Not I from pfCCNT1dE7-2 GFP into the Nru I–Not I site of pCMMP AMNNB. The HIV-1 tat was amplified from pSVtat by PCR using the following primers: 5′-AAC CGG TCT CGA GCC ACC ATG GAG CCA GTA GAT CCT AGA C-3′ and 5′-GGA TCC TCA GTC GTC ATC GTC TTT GTA GTC TTC CTT CGG GCC TGT CGG GTC-3′. The PCR product was cloned into the pSC-B (Stratagene, La Jolla, CA), and the Age I–Bam HI fragment from the cloned tat gene fragment was cloned into the Age I–Bam HI site of pCMMP KRAB IRES GFP, generating the pCMMP Tat. phLR/CMV was obtained from Promega.

2.4. Western blotting and immunoprecipitation

Western blotting and immunoprecipitation were performed according to previously described techniques (Shimizu et al., 2007; Urano et al., 2008). The following antibodies were used: anti-FLAG (F7425, Sigma), anti-CDK9 (100-401-167, Rockland), anti-HEXIM1 (ab25388, Abcam), anti-actin (MAB1501R, Millipore), and the EnVision+ system (Dako, Glostrup, Denmark).

2.5. Confocal microscopy

For imaging, NP2 cells in a well of a 48-well plate were co-transfected with 800 ng of pGFP-CCNT1 or pfCCNT1dE7-2 GFP along with 200 ng pHA-CDK9. Cells were grown on a whole slide glass (Matsunami Glass, Osaka, Japan) for 24 h, fixed in 4% formaldehyde in PBS for 5 min, permeabilized by 0.1% Triton-X 100 in PBS for 5–30 min, stained, mounted (Vectorshield, Vector Laboratories, Burlingame, CA), and imaged using a confocal microscope META 510 (Carl Zeiss, Tokyo, Japan). For the staining, fixed cells were incubated with Hoechst 33258 (Sigma), anti-HA polyclonal antibody (Sigma) followed by biotinylated anti-rabbit

goat antibody (GE Healthcare) and the streptoavidin conjugated with Alexa 555 (Invitrogen). Image brightness and contrast were processed by META510 software (Carl Zeiss).

2.6. Reporter assay

The luciferase activity was measured 48 h after transfection using a Steady-Glo or Dual-Glo assay kit (Promega) according to the manufacturer's protocol. The chemiluminescence was detected with the Veritas luminometer (Promega).

2.7. Viral production and infection

MLV vectors and HIV-1 were produced as described previously (Komano et al., 2004). To establish the NP2CD4CCR5 cells stably expressing fdE7-GFP, MLV was produced by using pCMMP fdE7-GFP.

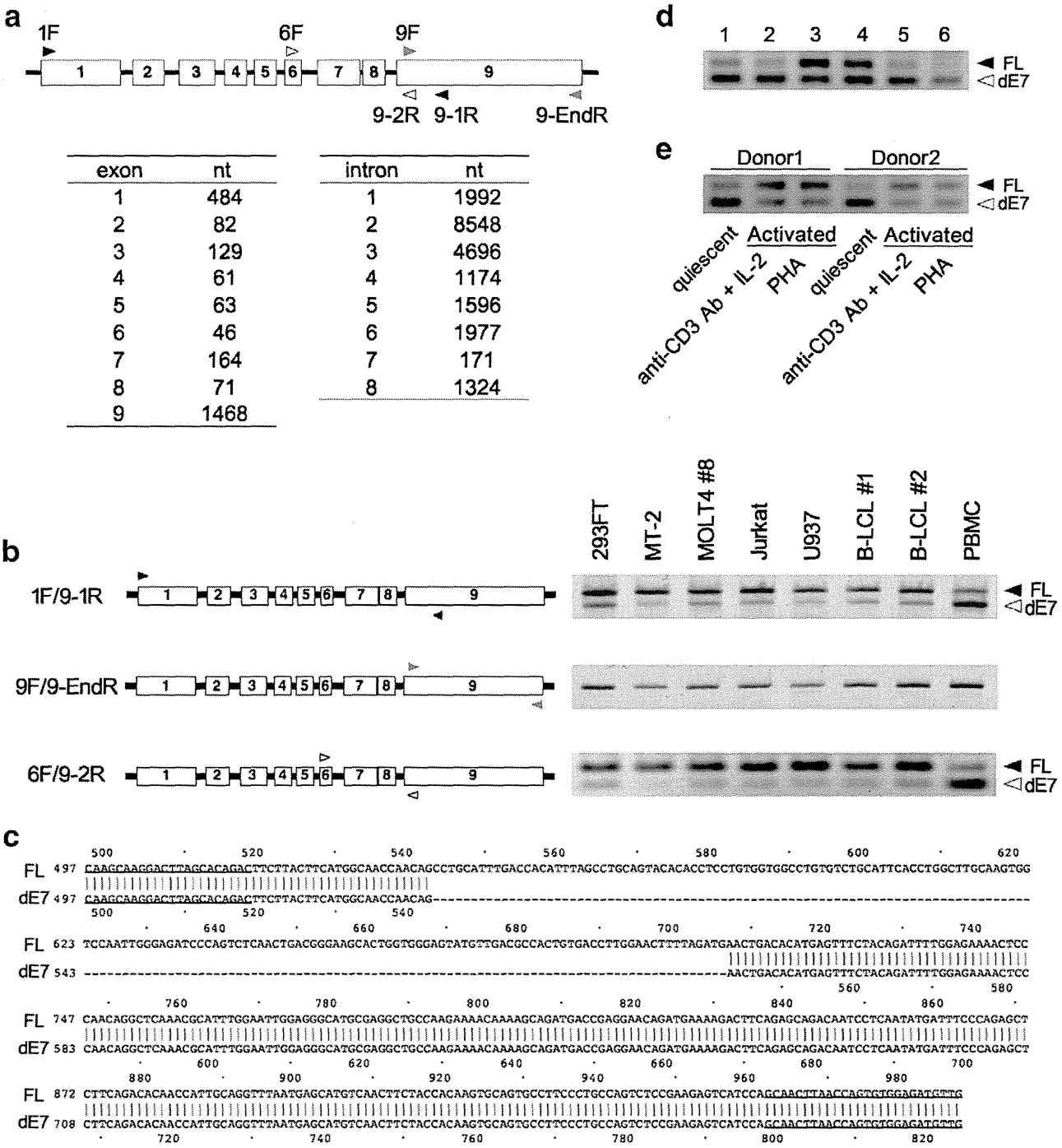

exon	nt
1	484
2	82
3	129
4	61
5	63
6	46
7	164
8	71
9	1468

intron	nt
1	1992
2	8548
3	4696
4	1174
5	1596
6	1977
7	171
8	1324

Fig. 1. Detection of the *CCNT1 dE7* transcript by RT-PCR. (a) Gene structure of *CCNT1*. The exons and introns are shown as boxes and lines, respectively. The binding sites for the primers used in this study are shown as arrowheads. Primer pairs are labeled with the same color. The nucleotide length of each exon or intron is given in the tables. (b) RT-PCR analysis using the 1F/9-1R, 9F/9-EndR and 6F/9-2R primer pairs. The upper and lower bands represent the *CCNT1 FL* and *dE7* transcripts (filled and open arrowheads, respectively). (c) Sequence comparison of the *CCNT1 FL* and *dE7* transcripts spanning the amplicon produced by the 6F/9-2R primers. The 5′ and 3′ underlined portions represent the 6F and 9-2R primer sequences. The number represents the nucleotide from the start codon. (d) RT-PCR analysis of six healthy donor-derived quiescent PBMC using the 6F/9-2R primer pair. The amplicons representing the *CCNT1 FL* and *dE7* transcripts are indicated by filled and open arrowheads, respectively. (e) RT-PCR analysis of two healthy donor-derived PBMC treated with a combination of anti-CD3 monoclonal antibody plus IL-2, or PHA, using the 6F/9-2R primer pair. The amplicons representing the *CCNT1 FL* and *dE7* transcripts are indicated by filled and open arrowheads, respectively.

For the negative control, pCMMP GFPf was used in place of pCMMP fdE7-GFP. The HIV-1_{HXB2} production assay, viral infection procedure and the monitoring HIV-1_{JR-CSL} replication are described previously (Komano et al., 2004; Shimizu et al., 2007).

3. Results and discussion

3.1. Identification of a novel splice variant of CCNT1 that lacks exon 7 (dE7)

RT-PCR analyses were conducted to amplify the 5′ half of the *CCNT1* open reading frame (ORF) using RNA extracted from various cell lines and healthy donor-derived naïve peripheral blood mononuclear cells (PBMC). The 1F and 9-1R primer set was used to amplify this region (Fig. 1a). Two amplicons were detected in all of the samples after agarose gel electrophoresis (Fig. 1b). The upper PCR amplicon had the mobility estimated from the ORF sequence (National Center for Biotechnology Information Accession AF048730.1), suggesting that it represents the intact *CCNT1* mRNA (Fig. 1a and b). The lower PCR amplicon was approximately 150 bp shorter than the *CCNT1 FL* transcript (Fig. 1b). By contrast, the 9F and 9-EndR primer set, which was designed to amplify the 3′ half of the *CCNT1* ORF, yielded one PCR amplicon in all of the samples, which had the electrophoretic mobility value estimated from the ORF sequence (Fig. 1b).

To more clearly separate the two amplicons generated by the former primer sets, a set of new primers was designed within exons 6 and 9 (6F and 9-2R, Fig. 1a). The presence of the shorter amplicon was confirmed with the new primer pair (Fig. 1b). Nucleotide sequencing revealed that the shorter amplicon was a *CCNT1* transcript lacking the entire exon 7 (*dE7*, Fig. 1c). The short amplicon was not a PCR artefact because it did not appear in PCR assays using the *CCNT1* cDNA as a template (data not shown). The splice variant *dE7* could be difficult to detect in Northern blot analyses because of small differences in lengths between the *CCNT1 FL* and *dE7* transcripts (Wei et al., 1998). PCR amplification efficiencies of the *dE7* transcript were slightly higher than those of the *FL* transcript (data not shown). Nevertheless, the PCR amplicon representing the *dE7* transcript was poorly detected in tissue culture cell lines (Fig. 1b). The *dE7/FL* transcript ratios were 0.4–0.6 in various cell lines according to the densitometric analysis. By contrast, the *dE7* amplicon level was almost equal to or more abundant than that of the *FL* amplicon in quiescent PBMC whereby the *dE7/FL* transcript ratios ranged from 0.9 to 2.2 (Fig. 1b and d). We assumed, thus, that the increased *dE7/FL* transcript ratio in quiescent PBMC might represent a low cellular proliferative potential when compared to established cell lines. To test this idea, the ratio of the two amplicons was examined in activated PBMC. When cells were exposed to a combination of anti-CD3 monoclonal antibody and IL-2, or to phytohemagglutinin (PHA), the *dE7/FL* transcript ratio decreased by 0.7- to 0.8-fold in two PBMC samples derived from two healthy donors (Fig. 1e). These data suggest that exon 7 skipping in the *CCNT1* transcript has an active role in regulating cell proliferation.

3.2. Regulation of dE7 transcript by nonsense-mediated decay (NMD)

The N-terminal portion of dE7 protein has the wild type amino acid sequence till the 180th residue (Asn). Exon 7 skipping results in a +1 frameshift at exon 8 that generates four aberrant amino acids, Arg–Thr–Asp–Thr, followed by a termination codon at the 11–13 nucleotide position of exon 8 (Fig. 2a). An abnormal mRNA has to be degraded rapidly because it may express an aberrant protein that could be harmful to the cell. The nonsense-mediated mRNA decay (NMD) system is responsible for the degradation of abnormal mRNAs (Stalder and Muhlemann, 2008). The NMD system recognizes a transcript bearing a premature termination codon (PTC). The PTC is a termination codon located more than approximately 50 nucleotides upstream of the last exon–exon junction. The termination codon of the *dE7* transcript is located 58 nucleotides upstream of the last exon–exon junction (Fig. 2a). Thus, the *dE7* transcript should be susceptible to NMD. The NMD system is translation-dependent. It has been reported that inhibition of translation leads to an accumulation of PTC-containing mRNAs (Carter et al., 1995). To examine whether the *dE7* transcript is susceptible to NMD, RT-PCR analyses were performed using RNA extracted from U937 cells treated with the protein synthesis inhibitor cycloheximide (CHX, Fig. 2b). Subsequently, the levels of the *dE7*, *FL*, and *c-myc* transcripts were examined. The levels of the *dE7* transcript substantially increased in the presence of CHX, whereas no significant change was observed for the *FL*, and *c-myc* transcripts (Fig. 2b). A kinase inhibitor wortmannin (WORT) has been shown to upmodulate PTC-containing transcripts by inhibiting the SMG1 function, a kinase that targets the key NMD effector UPF1 (Pal et al., 2001; Yamashita et al., 2001). The levels of the *dE7* transcript also increased dramatically in the presence of WORT (Fig. 2b). In contrast, no significant increment was observed for the *FL* and *c-myc* transcripts (Fig. 2b). Similar results were obtained with 293FT and MOLT4 cells (data not shown). Interestingly, the shift of *dE7-FL* transcript equilibrium to *dE7* in U937 cells by WORT resulted in the reduction of CCNT1 protein expression (Fig. 2c). Similar results were obtained in 293T cells (data not shown). This directly demonstrates that the exon skipping of CCNT1 exon 7 regulates the

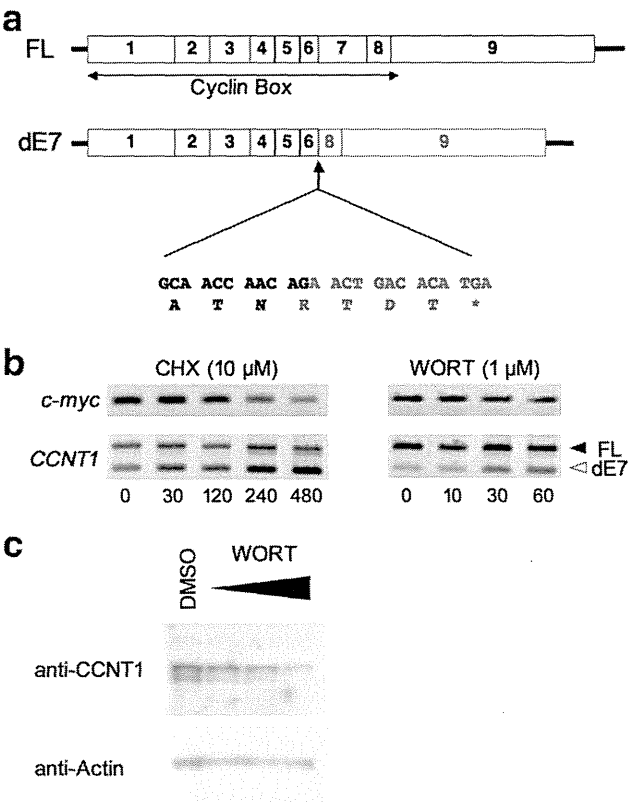

Fig. 2. Structure of the *CCNT1 dE7* transcript and its susceptibility to NMD. (a) Structure of the *CCNT1 FL* and *dE7* transcripts. The coding sequence is shown in the boxes, and the untranslated "exon" in the *dE7* transcript is shown in gray. The cyclin box, a part of CDK9-binding domain, is indicated (amino acids 1–254, arrow). The sequence for the exon 6–8 junction of *dE7* is shown, with the nucleotide and amino acid sequences derived from exon 6 and 8 represented in black and gray, respectively. The Asn (N) residue encoded by exon 6 corresponds to the 180th amino acid residue of CCNT1 protein. The asterisk represents the stop codon. (b) RT-PCR analysis of the *c-myc* and *CCNT1* transcripts in U937 cells using the 6F/9-2R primer pair. Cells were treated with 10 μM cycloheximide (CHX) or 1 μM wortmannin (WORT), and RNA was extracted from the cells at the indicated time points after drug exposure. The amplicons representing the *CCNT1 FL* and dE7 transcripts are indicated by filled and open arrowheads, respectively. (c) Effect of exon 7 skipping on CCNT1 protein expression. The correlation between *dE7/FL* transcript ratio and CCNT1 protein expression levels was analyzed by treating U937 cells with 50, 100, and 200 nM WORT for 16 h.

expression of CCNT1 protein. These data suggest that the *CCNT1 dE7* transcript is subjected to translation and the dE7 protein is expressed at certain levels, but the *dE7* transcript is recognized by NMD and degraded rapidly.

3.3. Expression profile of the dE7 transcript

The expression profile of the *dE7* transcript in various tissues was investigated. The *dE7* transcript was detected in almost all tissues examined (Fig. 3a). The *dE7/FL* transcript ratio was high in heart, brain, and skeletal muscle. These tissues generally do not contain actively proliferating cells. By contrast, the *dE7/FL* transcript ratio was low in placenta, liver, and pancreas. These tissues are intrinsically highly regenerative and contain actively proliferating cells under steady-state physiological conditions (Dor et al., 2004; Duncan et al., 2010). These data were in good agreement with the link between the *dE7/FL* transcript ratio and both the levels of CCNT1 protein expression and the cell proliferative potential (Figs. 1b and e and 2c). In blood cell fractions purified from a pooled blood of healthy donors, the dE7 transcript was more abundant in quiescent $CD4^+$, $CD8^+$, $CD14^+$, and $CD19^+$ cell fractions (Fig. 3b). The *dE7/FL* transcript ratio of PBMC decreased on treatment of cells with a mixture of PWM and Con A (Fig. 3b), consistent with the data presented in Fig. 1e. Similarly, the *dE7/FL* transcript ratio decreased in $CD19^+$ cell fractions activated by PWM (Fig. 3b). By contrast, the *dE7/FL* transcript ratio slightly increased in $CD4^+$ and $CD8^+$ cell fractions when cells were exposed to a mixture of Con A or PHA (Fig. 3b). It is likely that the reduction of the *dE7/FL* transcript ratio in activated PBMC partly reflects the $CD19^+$ cell fractions (Figs. 1e and 3b). These data suggest that the *dE7/FL* transcript ratio is subject to distinct regulation in different cell types. Our data indicate that cell growth stimulation lowers the *dE7/FL* transcript ratio in most cell types. Cell cycle progression requires a synthesis of a set of genes which depends on RNAPII–PTEF-b complex function. It seems reasonable that the cell growth potential correlates with the *dE7/FL*transcript ratio.

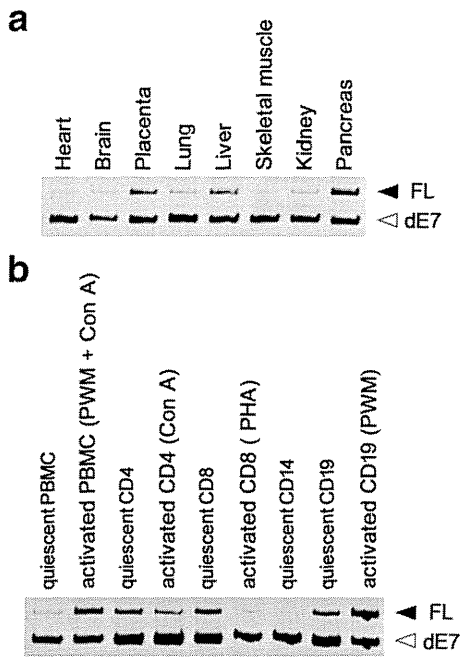

Fig. 3. Expression profiling of the *CCNT1 dE7* transcript in primary tissues and blood cell fractions using the 6F/9-2R primer pair. (a) RT-PCR analysis of various primary tissues under steady-state conditions using the 6F/9-2R primer pair. (b) RT-PCR analysis of blood cell fractions in quiescent or in activated conditions. The amplicons representing the *CCNT1 FL* and *dE7* transcripts are indicated by filled and open arrowheads, respectively.

3.4. Potential effect of dE7 protein on CCNT1 function

The NMD is coupled to the translation. Thus, the dE7 protein should be expressed at low levels. The cyclin box contains the CDK9-interaction domain of CCNT1 (amino acids 1–254). The *dE7* mRNA would produce an approximately 23 kDa protein that covers approximately 71% of the cyclin box of CCNT1 (amino acid 1–180; Fig. 2a). The X-ray crystallographic data and a biochemical study predict that dE7 protein retains the ability to interact with CDK9 (Baumli et al., 2008; Ivanov et al., 1999). Thus, a potential effect of dE7 protein on CCNT1 function was examined from the angle of its interaction with CDK9 by an expression vector, whereby dE7 was tagged with a FLAG epitope at the N-terminus, and with green fluorescence protein (GFP) at the C-terminus (fdE7-GFP). The expression of fdE7-GFP was confirmed by Western blot analyses using anti-FLAG, anti-CCNT1, and anti-GFP antibodies (data not shown, partly shown in Figs. 4b and 5d). The intracellular distribution of fdE7-GFP was examined in NP2 cells and compared with that of GFP-CCNT1. Consistent to the previous report, the GFP-CCNT1 and hemagglutinin-tagged CDK9 (HA-CDK9) co-distributed to the nuclear matrix-attached speckle-domains (Fig. 4a), which are known to be the sites for the RNA Pol II-mediated transcription

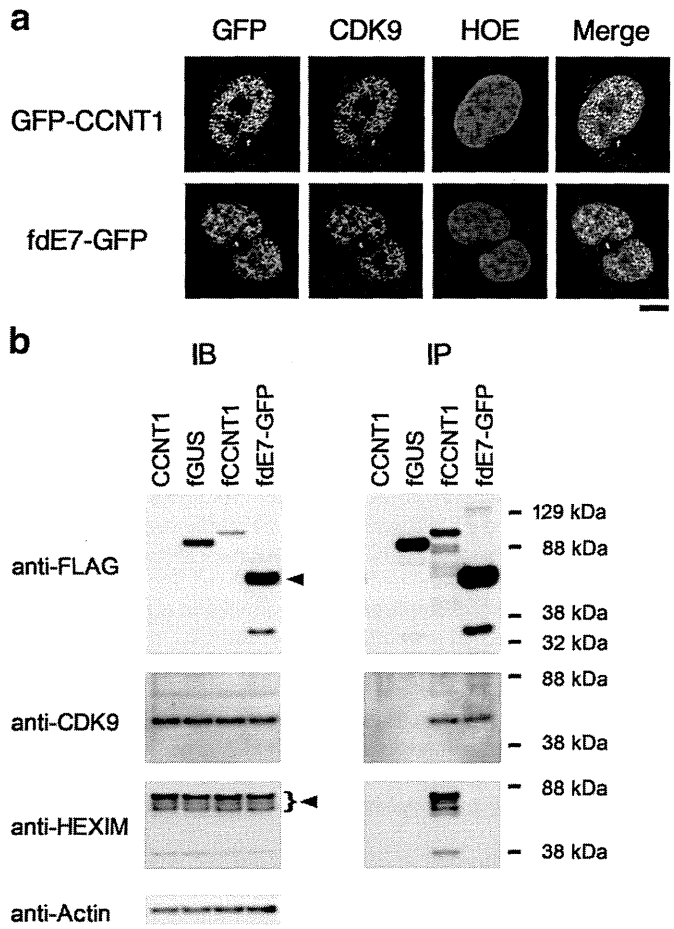

Fig. 4. Analysis of the CCNT1 dE7 protein. (a) The confocal microscopy images of NP2 cells expressing GFP-CCNT1 or fdE7-GFP along with HA-CDK9. The green, red, and blue represent the GFP, the HA-CDK9 visualized by using anti-HA antibodies, and the Hoechst 33258-stained nucleus, respectively. Magnification, ×630; scale bar, 10 μm. (b) The 293FT cells were transfected with expression plasmids for untagged-CCNT1 (CCNT1), FLAG-tagged beta-glucuronidase (fGUS), fCCNT1, and fdE7-GFP. Subsequently, Western blot (IB) and co-immunoprecipitation (IP) analyses were performed. The bands representing fdE7-GFP and HEXIM1 are indicated by arrowheads. The anti-FLAG antibody was used for IP. The primary antibodies for the IB are indicated on the left. The untagged-CCNT1 and fGUS were used as negative controls.

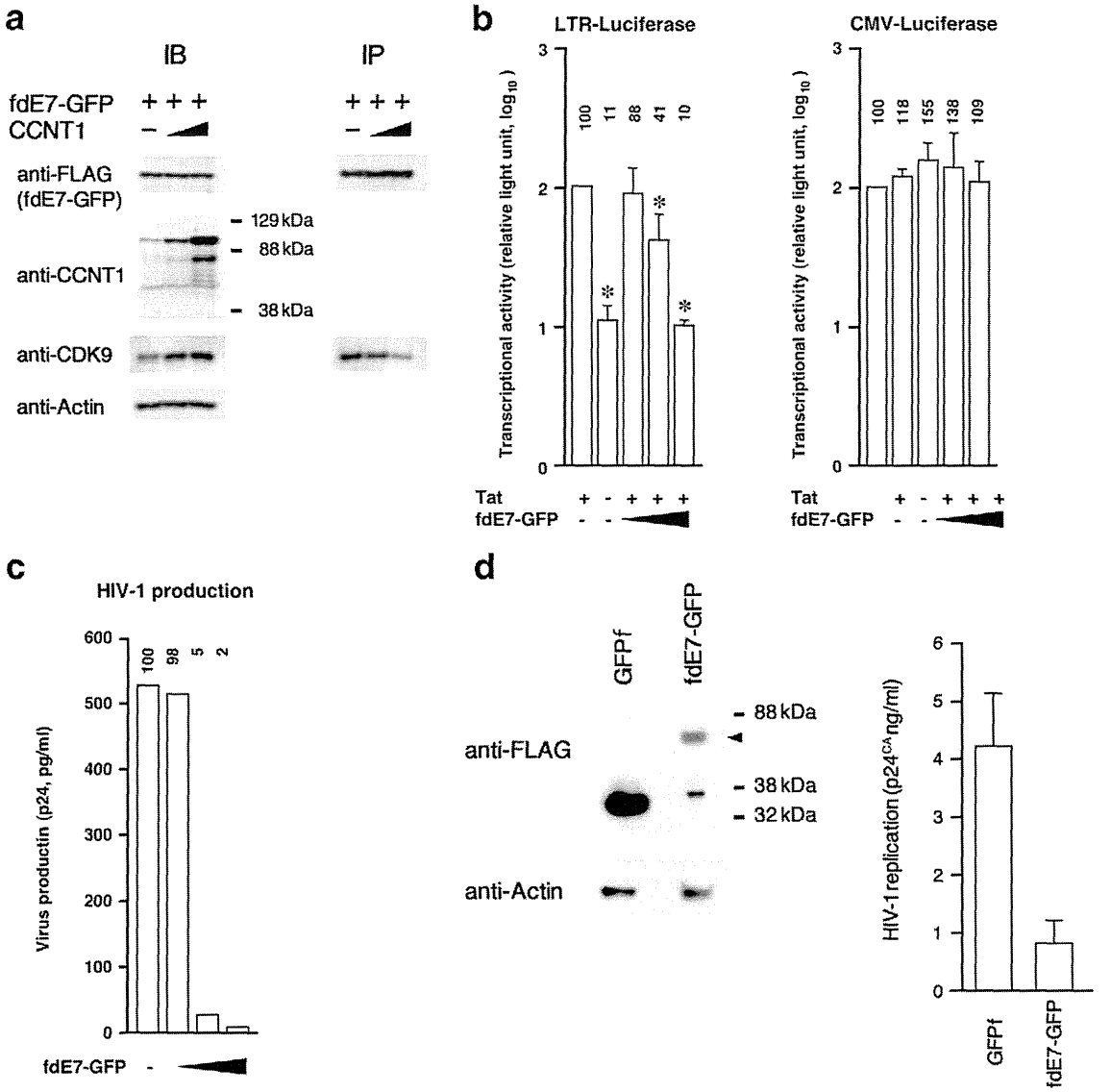

Fig. 5. Biological function of fdE7-GFP. Competition co-immunoprecipitation assay between fdE7-GFP and CCNT1 for CDK9. The 293FT cells were transfected with expression plasmids for fdE7-GFP, HA-CDK9 along with increasing amount of untagged-CCNT1 (CCNT1). Subsequently, Western blot (IB) and co-immunoprecipitation (IP) analyses were performed. The anti-FLAG antibody was used for IP. The primary antibodies for the IB are indicated on the left. (b) The effect of fdE7-GFP expression on the HIV-1 Tat/LTR-driven transcription. The luciferase-expressing reporter plasmids were transfected into 293T cells grown in a 48-well plate. For transfection, either 20 ng of pLTR-Luc (LTR-Luciferase) or phRL/CMV (CMV-Luciferase) was co-transfected with 100 ng of pCMMP Tat and the increasing amount of pMAT fdE7-GFP (40, 200, and 1000 ng), respectively. The total amount of plasmid DNA to transfect into cells was adjusted by pMAT fGUS. The luciferase expression levels with Tat without fdE7-GFP were set as 100% (first lane, control). The average and standard deviation from four and two independent experiments for LTR and CMV constructs, respectively, are shown. Statistical significance of the given data against the control was analyzed by two-tailed Student's *t*-test (asterisk, $P<0.05$). (c) The effect of fdE7-GFP expression on the HIV-1 production. Viral production was assessed by transfecting 200 ng of proviral DNA pHXB2 along with increasing amount of pMAT fdE7-GFP (40, 200, and 1000 ng) into 293T cells grown in a 6-well plate and the viral capsid protein ($p24^{CA}$) levels in the culture supernatant were measured by ELISA at 2 days-post transfection. The level of HIV-1 production relative to the no fdE7-GFP control (first lane) was indicated. (d) Ectopic constitutive expression of fdE7-GFP in NP2CD4CCR5 cells delayed the replication of HIV-$1_{JR\text{-}CSF}$. Expression of GFPf and fdE7-GFP (arrowhead) was verified by Western blot analysis. Cells grown in a 96-well plate were infected with HIV-$1_{JR\text{-}CSF}$ (ca. 162 pg $p24^{CA}$/ well) and the $p24^{CA}$ levels in the culture supernatant were measured by ELISA at 4 days post-infection. The average and standard deviation from triplicated wells are shown.

and the co-transcriptional pre-mRNA processing that P-TEFb complex is involved (Herrmann and Mancini, 2001; Urano et al., 2008). The fdE7-GFP was mainly detected in the nucleus. In the nucleus, the fdE7-GFP accumulated in the discrete speckle compartments and showed the co-distribution with HA-CDK9 similar to GFP-CCNT1 or CCNK (Fig. 4a) (Urano et al., 2008). Co-immunoprecipitation analyses showed that fdE7-GFP interacted with CDK9, the essential component of P-TEFb complex, but not with HEXIM1, the negative regulator of P-TEFb complex, consistent with the previous report (Fig. 4b and (Barboric et al., 2007)). By contrast, the FL CCNT1 interacted only with both CDK9 and HEXIM1 (Fig. 4b). Note that a few bands were detected on the Western blot for HEXIM1 due to its modification variants, as reported previously (Byers et al., 2005). These data suggest that dE7 is able to dysregulate the function of the P-TEFb complex by competing with FL CCNT1 for CDK9. The dE7 protein lacks the domains responsible for the association with Brd4 and HIV-1 Tat (Jang et al., 2005; Wei et al., 1998). Thus, we did not examine the physical interaction between dE7 protein with these factors.

The function of dE7 protein was examined further. The competitive co-immunoprecipitation assay revealed that the CDK9–fdE7-GFP interaction was disrupted by increasing amounts of FL CCNT1 (Fig. 5a). This supports the above hypothesis. Note that the expression of FL CCNT1 increased the levels of CDK9, presumably because the excess CCNT1 stabilized the CDK9 by binding (Fig. 5a, left

panel, anti-CDK9). The effect of dE7 on transcription was examined by the luciferase reporter assay. The Tat-dependent transcription from HIV-1 LTR promoter is heavily dependent on P-TEFb complex (Wei et al., 1998; Zhou and Yik, 2006). In agreement with the above hypothesis, the HIV-1 Tat/LTR-driven luciferase activity was decreased in the presence of fdE7-GFP in a dose-dependent manner (Fig. 5b). This effect was not observed in the CMV promoter-driven luciferase reporter plasmid (Fig. 5b). Consistent to these observations, HIV-1 production was inhibited by fdE7-GFP in a co-transfection assay using a proviral DNA (Fig. 5c). Furthermore, HIV-1 replication was inhibited in NP2CD4CCR5 cells constitutively expressing fdE7-GFP (Fig. 5d). Similar observations were made in Lusiv cells (data not shown). Collectively, it is suggested that dE7 protein inhibits FL CCNT1 dominant-negatively.

4. Conclusions

In this report, we described a novel splice variant of *CCNT1*, named *dE7*, which is generated by exon skipping. The expression levels of *CCNT1 FL* are tightly regulated, since *CCNT1* synthesis is rate-limiting for the formation of the P-TEFb complex (Haaland et al., 2003). We therefore propose that, in the steady-state, the *CCNT1* transcript primarily undergoes exon 7 skipping to self-limit CCNT1 expression. When cells are exposed to a growth signal, exon skipping is suppressed and CCNT1 is synthesized. It is possible that this mechanism partly accounts for the post-transcriptional regulation of *CCNT1* expression, which was reported previously (Herrmann et al., 1998; Liou et al., 2002, 2006; Sung and Rice, 2006). The dE7 protein was shown to act as a dominant-negative inhibitor of the FL CCNT1 by competing for CDK9. The P-TEFb complex plays a critical role in HIV-1 LTR/Tat-driven transcription, which was strongly inhibited by dE7 protein. This dominant-negative effect of dE7 protein on FL CCNT1 might be another layer to self-limit the CCNT1 function. It might be also a safe-guard mechanism to protect against a failure of NMD to degrade the *dE7* transcript completely. It is noted that expression of the dE7 protein was undetectable as long as commercially available antibodies recognizing the CCNT1 N-terminus were used that detected FL protein only weakly (data not shown) unless it was fused to GFP (data not shown), suggesting that the native dE7 protein could be unstable. It is reasonable that a protein bearing a dominant negative transcriptional effect, such as dE7 protein, has a short half life to achieve a prompt response to cell growth stimuli.

This ubiquitously expressed *dE7* transcript was abundant in quiescent cells, but scarce in actively proliferating cells. The *dE7/FL* transcript ratio could be a sensitive predictor of cellular proliferative potential, and it could have applications for the diagnosis of malignancies.

The molecular mechanism has been yet to be clarified by which the exon 7 skipping is regulated in *CCNT1* mRNA. Polypyrimidine tract binding proteins, including PTB, play a suppressive role in alternative splicing (Sawicka et al., 2008; Spellman et al., 2005). Three polypyrimidine tracts are located in the *CCNT1* intron 6 proximal to exon 7, suggesting that PTB and related factors may be involved in the regulation of exon 7 skipping. However, overexpression of PTB did not affect the *dE7/FL* transcript ratio in 293T cells (data not shown). Further analysis is required to fully understand the mechanism that regulates *CCNT1* exon 7 skipping. A recent computational analysis revealed that one-third of alternative transcripts contain PTCs that can be recognized by NMD, suggesting that the expression levels of certain proteins were globally regulated by alternative splicing and NMD (Lewis et al., 2003). Our results suggest that *CCNT1* may be one of these proteins.

Acknowledgements

This work was supported by the Japan Health Science Foundation, the Japanese Ministry of Health, Labor, and Welfare (H18-AIDS-W-003 to J.K.), and the Japanese Ministry of Education, Culture, Sports, Science and Technology (18689014 and 18659136 to J.K.). E.U., K.M., R.I., Y.F., and J.K. designed and performed experiments and interpreted the data. J.K. wrote the manuscript. All authors declare no potential competing financial interests.

References

Barboric, M., et al., 2007. Tat competes with HEXIM1 to increase the active pool of P-TEFb for HIV-1 transcription. Nucleic Acids Res. 35, 2003–2012.
Barboric, M., Lenasi, T., Chen, H., Johansen, E.B., Guo, S., Peterlin, B.M., 2009. 7SK snRNP/P-TEFb couples transcription elongation with alternative splicing and is essential for vertebrate development. Proc. Natl. Acad. Sci. U. S. A. 106, 7798–7803 (Epub 2009 Apr 27).
Baumli, S., et al., 2008. The structure of P-TEFb (CDK9/cyclin T1), its complex with flavopiridol and regulation by phosphorylation. EMBO J. 27, 1907–1918 (Epub 2008 Jun 19).
Bres, V., Yoh, S.M., Jones, K.A., 2008. The multi-tasking P-TEFb complex. Curr. Opin. Cell Biol. 20, 334–340 Epub 2008 May 29.
Bres, V., Yoshida, T., Pickle, L., Jones, K.A., 2009. SKIP interacts with c-Myc and Menin to promote HIV-1 Tat transactivation. Mol. Cell 36, 75–87.
Byers, S.A., Price, J.P., Cooper, J.J., Li, Q., Price, D.H., 2005. HEXIM2, a HEXIM1-related protein, regulates positive transcription elongation factor b through association with 7SK. J. Biol. Chem. 280, 16360–16367 (Epub 2005 Feb 14).
Carter, M.S., et al., 1995. A regulatory mechanism that detects premature nonsense codons in T-cell receptor transcripts in vivo is reversed by protein synthesis inhibitors in vitro. J. Biol. Chem. 270, 28995–29003.
De Falco, M., De Luca, A., 2006. Involvement of cdks and cyclins in muscle differentiation. Eur. J. Histochem. 50, 19–23.
De Falco, G., et al., 2005. Cdk9 regulates neural differentiation and its expression correlates with the differentiation grade of neuroblastoma and PNET tumors. Cancer Biol. Ther. 4, 277–281 (Epub 2005 Mar 20).
De Falco, G., et al., 2008. Cdk9/Cyclin T1 complex: a key player during the activation/differentiation process of normal lymphoid B cells. J. Cell. Physiol. 215, 276–282.
Dor, Y., Brown, J., Martinez, O.I., Melton, D.A., 2004. Adult pancreatic beta-cells are formed by self-duplication rather than stem-cell differentiation. Nature 429, 41–46.
Duncan, A.W., et al., 2010. The ploidy conveyor of mature hepatocytes as a source of genetic variation. Nature 467, 707–710 (Epub 2010 Sep 22).
Elagib, K.E., et al., 2008. Cross-talk of GATA-1 and P-TEFb in megakaryocyte differentiation. Blood 112, 4884–4894 (Epub 2008 Sep 9).
Garriga, J., Grana, X., 2004. Cellular control of gene expression by T-type cyclin/CDK9 complexes. Gene 337, 15–23.
Garriga, J., Peng, J., Parreno, M., Price, D.H., Henderson, E.E., Grana, X., 1998. Upregulation of cyclin T1/CDK9 complexes during T cell activation. Oncogene 17, 3093–3102.
Haaland, R.E., Herrmann, C.H., Rice, A.P., 2003. Increased association of 7SK snRNA with Tat cofactor P-TEFb following activation of peripheral blood lymphocytes. AIDS 17, 2429–2436.
Herrmann, C.H., Mancini, M.A., 2001. The Cdk9 and cyclin T subunits of TAK/P-TEFb localize to splicing factor-rich nuclear speckle regions. J. Cell Sci. 114, 1491–1503.
Herrmann, C.H., Carroll, R.G., Wei, P., Jones, K.A., Rice, A.P., 1998. Tat-associated kinase, TAK, activity is regulated by distinct mechanisms in peripheral blood lymphocytes and promonocytic cell lines. J. Virol. 72, 9881–9888.
Ivanov, D., Kwak, Y.T., Nee, E., Guo, J., Garcia-Martinez, L.F., Gaynor, R.B., 1999. Cyclin T1 domains involved in complex formation with Tat and TAR RNA are critical for tat-activation. J. Mol. Biol. 288, 41–56.
Jang, M.K., Mochizuki, K., Zhou, M., Jeong, H.S., Brady, J.N., Ozato, K., 2005. The bromodomain protein Brd4 is a positive regulatory component of P-TEFb and stimulates RNA polymerase II-dependent transcription. Mol. Cell 19, 523–534.
Komano, J., Miyauchi, K., Matsuda, Z., Yamamoto, N., 2004. Inhibiting the Arp2/3 complex limits infection of both intracellular mature vaccinia virus and primate lentiviruses. Mol. Biol. Cell 15, 5197–5207.
Leucci, E., et al., 2007. The role of the Cdk9/Cyclin T1 complex in T cell differentiation. J. Cell. Physiol. 212, 411–415.
Lewis, B.P., Green, R.E., Brenner, S.E., 2003. Evidence for the widespread coupling of alternative splicing and nonsense-mediated mRNA decay in humans. Proc. Natl. Acad. Sci. U. S. A. 100, 189–192 (Epub 2002 Dec 26).
Liou, L.Y., Herrmann, C.H., Rice, A.P., 2002. Transient induction of cyclin T1 during human macrophage differentiation regulates human immunodeficiency virus type 1 Tat transactivation function. J. Virol. 76, 10579–10587.
Liou, L.Y., Haaland, R.E., Herrmann, C.H., Rice, A.P., 2006. Cyclin T1 but not cyclin T2a is induced by a post-transcriptional mechanism in PAMP-activated monocyte-derived macrophages. J. Leukoc. Biol. 79, 388–396 (Epub 2005 Dec 5).
Marshall, R.M., Grana, X., 2006. Mechanisms controlling CDK9 activity. Front. Biosci. 11, 2598–2613.
Marshall, R.M., Salerno, D., Garriga, J., Grana, X., 2005. Cyclin T1 expression is regulated by multiple signaling pathways and mechanisms during activation of human peripheral blood lymphocytes. J. Immunol. 175, 6402–6411.
Nguyen, V.T., Kiss, T., Michels, A.A., Bensaude, O., 2001. 7SK small nuclear RNA binds to and inhibits the activity of CDK9/cyclin T complexes. Nature 414, 322–325.
Pal, M., Ishigaki, Y., Nagy, E., Maquat, L.E., 2001. Evidence that phosphorylation of human Upf1 protein varies with intracellular location and is mediated by a wortmannin-sensitive and rapamycin-sensitive PI 3-kinase-related kinase signaling pathway. RNA 7, 5–15.

Peterlin, B.M., Price, D.H., 2006. Controlling the elongation phase of transcription with P-TEFb. Mol. Cell 23, 297–305.
Pirngruber, J., Shchebet, A., Johnsen, S.A., 2009. Insights into the function of the human P-TEFb component CDK9 in the regulation of chromatin modifications and co-transcriptional mRNA processing. Cell Cycle 8, 3636–3642 (Epub 2009 Nov 24).
Rechter, S., et al., 2009. Cyclin-dependent kinases phosphorylate the cytomegalovirus RNA export protein pUL69 and modulate its nuclear localization and activity. J. Biol. Chem. 284, 8605–8613 (Epub 2009 Jan 29).
Sawicka, K., Bushell, M., Spriggs, K.A., Willis, A.E., 2008. Polypyrimidine-tract-binding protein: a multifunctional RNA-binding protein. Biochem. Soc. Trans. 36, 641–647.
Shimizu, S., et al., 2007. Inhibiting lentiviral replication by HEXIM1, a cellular negative regulator of the CDK9/cyclin T complex. AIDS 21, 575–582.
Spellman, R., et al., 2005. Regulation of alternative splicing by PTB and associated factors. Biochem. Soc. Trans. 33, 457–460.
Stalder, L., Muhlemann, O., 2008. The meaning of nonsense. Trends Cell Biol. 18, 315–321 (Epub 2008 Jun 2).
Sung, T.L., Rice, A.P., 2006. Effects of prostratin on Cyclin T1/P-TEFb function and the gene expression profile in primary resting CD4 + T cells. Retrovirology 3, 66.
Sung, T.L., Rice, A.P., 2009. miR-198 inhibits HIV-1 gene expression and replication in monocytes and its mechanism of action appears to involve repression of cyclin T1. PLoS Pathog. 5, e1000263 (Epub 2009 Jan 16).
Urano, E., et al., 2008. Cyclin K/CPR4 inhibits primate lentiviral replication by inactivating Tat/positive transcription elongation factor b-dependent long terminal repeat transcription. AIDS 22, 1081–1083.
Urano, E., Ichikawa, R., Morikawa, Y., Yoshida, T., Koyanagi, Y., Komano, J., 2010. T cell-based functional cDNA library screening identified SEC14-like 1a carboxy-terminal domain as a negative regulator of human immunodeficiency virus replication. Vaccine 28, B68–B74.
Wei, P., Garber, M.E., Fang, S.M., Fischer, W.H., Jones, K.A., 1998. A novel CDK9-associated C-type cyclin interacts directly with HIV-1 Tat and mediates its high-affinity, loop-specific binding to TAR RNA. Cell 92, 451–462.
Yamashita, A., Ohnishi, T., Kashima, I., Taya, Y., Ohno, S., 2001. Human SMG-1, a novel phosphatidylinositol 3-kinase-related protein kinase, associates with components of the mRNA surveillance complex and is involved in the regulation of nonsense-mediated mRNA decay. Genes Dev. 15, 2215–2228.
Yang, Z., Zhu, Q., Luo, K., Zhou, Q., 2001. The 7SK small nuclear RNA inhibits the CDK9/cyclin T1 kinase to control transcription. Nature 414, 317–322.
Yang, Z., He, N., Zhou, Q., 2008. Brd4 recruits P-TEFb to chromosomes at late mitosis to promote G1 gene expression and cell cycle progression. Mol. Cell. Biol. 28, 967–976 (Epub 2007 Nov 26).
Zhou, Q., Yik, J.H., 2006. The Yin and Yang of P-TEFb regulation: implications for human immunodeficiency virus gene expression and global control of cell growth and differentiation. Microbiol. Mol. Biol. Rev. 70, 646–659.

Biochemical and Biophysical Research Communications 424 (2012) 519–523

Contents lists available at SciVerse ScienceDirect

Biochemical and Biophysical Research Communications

journal homepage: www.elsevier.com/locate/ybbrc

Toll-like receptor (TLR) 3 as a surrogate sensor of retroviral infection in human cells

Kosuke Miyauchi [a,d], Emiko Urano [a], Satoshi Takeda [a], Tsutomu Murakami [a], Yoshiaki Okada [b], Kui Cheng [c], Hang Yin [c], Masato Kubo [d,e], Jun Komano [a,*]

[a] AIDS Research Center, National Institute of Infectious Diseases, 1-23-1 Toyama, Shinjuku, Tokyo 162-8640, Japan
[b] Division of Safety Research on Blood and Biological Products, National Institute of Infectious Diseases, 4-7-1 Murayama, Tokyo 208-0011, Japan
[c] Department of Chemistry and Biochemistry, University of Colorado at Boulder, Boulder, CO 80309-0215, United States
[d] Research Center for Allergy and Immunology, RIKEN Yokohama Institute, 1-7-22 Suehiro-cho, Tsurumi, Yokohama, Kanagawa 230-0045, Japan
[e] Division of Molecular Pathology, Research Institute for Biological Sciences, Tokyo University of Sciences, 2669 Yamazaki, Noda, Chiba 278-0022, Japan

ARTICLE INFO

Article history:
Received 20 June 2012
Available online 4 July 2012

Keywords:
Human
Cytokines
Signal Transduction
Viral infections (major category)
Toll-like receptor (TLR)
Retrovirus
Interferon gamma-induced protein 10 (IP-10)/CXCL10

ABSTRACT

The toll-like receptor (TLR)-7 has been shown to sense the retroviral infection. However, a surrogate sensor has been implicated. We examined whether retrovirus serves as a TLR3 ligand in human cells by utilizing cell lines LNCaP and PC-3 lacking TLR7, and the xenotropic murine leukemia virus-relamoted virus (XMRV) insensitive to human tripartite motif-containing (TRIM) 5, a newly characterized pattern recognition receptor (PRR). A dominant-negative TLR3 or a chemical inhibitor of TLR3 attenuated the XMRV-induced IP-10/CXCL10 expression, a marker of TLR3 response. These data clearly indicated that retroviral infection exemplified by XMRV activates the TLR3 signal in human cells.

1. Introduction

The pattern recognition receptor (PRR) plays a key role in the innate immune response to microbial infection [1,2]. Viral RNA can serve as a ligand for the PRR system. Such RNA sensors are present in both endosomes (for example, toll-like receptor (TLR)-3 and -7, double and single-stranded RNA sensors, respectively) and cytoplasm (for example, retinoic acid-inducible gene-I, RIG-I; melanoma differentiation associated gene-5, MDA5). TLR3 is also known to be expressed on the cell surface of epithelial origin [3]. The use of RNA sensors in host defense against retroviral infection remains controversial.

Retroviruses are enveloped viruses with single-stranded RNA genomes. Retroviruses replicate using a unique strategy to protect the viral genomic RNA from being recognized by host RNA sensors. In the production phase of the retroviral life cycle, transcription from proviral DNA integrated into the host chromosome occurs via a mechanism that is essentially identical to that of transcription of cellular genes. The accumulation levels of viral transcript in the infected cells are modest relative to other RNA viruses encoding their own RNA polymerases to amplify viral RNA. In this sense, the mRNA of proviral DNA is barely distinguishable from mRNA transcribed from cellular genes unless the viral RNA has some sequences that evoke anti-viral responses [4,5], which does not apply to all the retroviral species. No evidence has been reported whether the TLR3/7-mediated signal is activated by retroviral RNA transcribed from the provirus. The retroviral genome is not exposed to the surface of virion. Thus, the recognition of retroviral genomic RNA at the cell surface appears unlikely. In the entry phase, the viral genome released into the cytoplasm after the virus-cell membrane fusion is packed in the core. The reverse transcription of viral genome takes place in the cytoplasm and the reverse-transcribed viral DNA is mostly covered with proteins forming the preintegration complex (PIC) [6]. Thus, the exposure of viral genome to the cytoplasmic viral RNA sensor appears limited. Thus, the reverse-transcribed viral DNA may not serve as an efficient ligand for cytoplasmic DNA sensors, such as the DNA-dependent activator of interferon regulatory factor (DAI).

A fraction of retroviral particles, either infectious or non-infectious, are actively endocytosed and degraded in the endosome/lysosome, providing the viral genome as a ligand for RNA sensors, namely a single-stranded RNA sensor TLR7 [7–11]. This model has been tested directly in dendritic cell/human immunodeficiency

Abbreviations: AZT, azidothymidine; dnTLR, dominant negative TLR; PIC, preintegration complex; TRIM, tripartite motif-containing.

* Corresponding author. Address: Osaka Prefectural Institute of Public Health, Dept. of Infectious Diseases, Virology Division, 3-69, Nakamachi, 1-chome, Higashinari-ku, Osaka 537-0025, Japan. Fax: +81-6-6972-2393.
E-mail addresses: ajkomano@nih.go.jp, komano@iph.pref.osaka.jp (J. Komano).

0006-291X/$ - see front matter © 2012 Elsevier Inc. All rights reserved.
http://dx.doi.org/10.1016/j.bbrc.2012.06.148

virus type 1 (HIV-1) systems [7]. Human T-cell luekemia virus type 1 (HTLV-1) has been also shown to activate TLR7-mediated signal [12]. Not only TLR7, TLR8 and TLR9 have been involved in the recognition of retroviruses [7,9]. Interestingly, the retroviral infection still evokes some host immune response in the absence of TLR7, suggesting a surrogate sensor of retroviral infection [7,9,10]. It has been reported that HIV-based lentiviral vectors evoke signals from TLR3 as well as TLR7 in mouse cells [1]. However, the involvement of TLR3 in the recognition of infecting retroviral genomes remains to be clarified in human cells.

The retroviral genome is predicted to dimerize and form an extensive secondary structure [13–15]. In these processes, it is likely that double-stranded RNA, a ligand of TLR3, is formed. We hypothesized that retroviruses can potentially activate TLR3 during the viral entry phase. In this study, we demonstrated definitively that TLR3 is a sensor of retroviral genome in human cells through a genetic and a chemical biology approaches.

2. Materials and methods

2.1. Tissue culture

Cells were maintained in RPMI 1640 medium (Sigma, St. Louis, MO) supplemented with 10% fetal bovine serum (Japan Bioserum, Tokyo, Japan), 50 U/ml penicillin and 50 μg/ml streptomycin (Invitrogen, Tokyo, Japan) at 37 °C in a humidified 5% CO_2 atmosphere. 22RV-1 and LNCaP (clone FGC) were obtained from Dainippon Sumitomo Pharma Biomedical (Osaka, Japan), while PC-3 and DU145 were obtained from the National Institute of Radiological Sciences. AZT was obtained from the NIH AIDS Research and Reference Reagent Program. The TLR3 ligand, poly(I:C12U), was used at a concentration of 25 μg/ml (Hemispherx Biopharma, Philadelphia, PA). Imiquimod (Sigma) was used at a concentration of 40 μM. The TLR3 inhibitor 4a has been described previously [16].

2.2. Cytokine measurement

The levels of IP-10/CXCL10 were measured using Quantikine IP-10 ELISA kit for the most of the data (R&D Systems, Minneapolis, MN), except 23-Plex panel of the Bioplex cytokine assay system was used for the experiment in Fig. 1D (Bio-Rad Laboratories, Hercules, CA).

2.3. Virus

The xenotropic murine leukemia virus-relamoted virus (XMRV) was prepared from the tissue culture supernatant of 22RV-1 cells. Tissue culture supernatants of 22RV-1 cells were passed through nitrocellulose filters (0.45 μm) and the virions were collected by centrifugation over 20% (w/w) sucrose/PBS (Optima™ L-70 k, SW 55 Ti rotor, 11 k × *g* for 2 h; Beckman Coulter, Miami, FL). The pellet was resuspended in tissue culture medium to 1/10–20 the original volume. Approximately 5% of LNCaP cells were infected with XMRV at 2 days-postinfection as determined by immunofluorescent assay using anti-R-MuLV p30 (Gag) polyclonal serum (NCI BCB repository, 81S263). The MuLV vector was produced as described previously [17]. Replication of XMRV was measured by assessing RT acitivity using the EnzChek Reverse Transcriptase Assay kit (Invitrogen).

2.4. Western blotting

Western blotting was performed as described previously [18]. The following probes were used: an anti-hemagglutinin (HA) monoclonal antibody 6E2 (Cell Signaling Technology, Beverly, MA); an anti-actin monoclonal antibody 1501R (Millipore); and a biotin conjugated secondary antibody and streptavidin conjugated with horseradish peroxidase (HRP, GE Healthcare, Tokyo, Japan).

2.5. RT-PCR

Total RNA from LNCaP cells was isolated using the SV Total RNA Isolation System (Promega, Madison, WI). RT-PCR was carried out using the OneStep RT-PCR Kit (Qiagen, Valencia, CA) using the following primers: TLR3, 5′-TGG TTG GGC CAC CTA GAA GTA-3′ and 5′-TCT CCA TTC CTG GCC TGT G-3′; TLR7, 5′-TTT ACC TGG ATG GAA ACC AGC TA-3′ and 5′-TCA AGG CTG AGA AGC TGT AAG CTA-3′; IP-10/CXCL10, 5′-TTC AAG GAG TAC CTC TCT CTA G-3′ and 5′-CTG GAT TCA GAC ATC TCT TCT C-3′; GAPDH for Fig. 1A, 5′-GTG GAA GGA CTC ATG ACC ACA GTC-3′ and 5′-CAT GTG GGC CAT GAG GTC CAC CAC-3′; and GAPDH for Fig. 2B, 5′-GTC GGA GTC AAG GAT TTG-3′ and 5′-TGG TGG AAT CAT ATT GGA A-3′.

2.6. Cloning

The cDNA library of human PBMCs was used as a template (Takara, Otsu, Japan). The following primers were used: forward, 5′-AGC GGC CGC ACC ATG AGA CAG ACT TTG CCT TGT ATC TAC TTT TGG-3′ and reverse, 5′-AAC CGG TTA GGC GTA GTC TGG CAC ATC ATA GGG GTA AAA CTG TTC TGT CTG TCT GTC TAT TTC TTT G-3′. The reverse primer contained the HA tag sequence. The PCR fragment spanning the ectodomain and transmembrane domain of tlr3 was cloned into NotI-AgeI sites of pQcXIP (Clontech, Palo Alto, CA). The pQcXIP without an insert was used as a control for pQcdnTLR3. The LNCaP cells were infected with the MuLV vector and selected with 1.0 μg/ml puromycin.

3. Results and discussion

To clearly differentiate the TLR3 signal from TLR7 in human cells, we carefully chose the experimental system. The prostate cancer cell lines LNCaP and PC-3 have been chosen for cells because they expressed TLR3 endogenously but not TLR7 [19]. We verified the lack of TLR7 expression by RT-PCR in these cell lines in agreement with the previous report (Fig. 1A) [19]. We chose XMRV because this retrovirus is not restricted by a newly-identified PRR protein human tripartite motif-containing (TRIM) 5 [20–22]. The exposure of LNCaP cells to bacteria-derived plasmid DNA induced the robust production of a PRR-responsive cytokine, namely interferon gamma-induced protein 10 (IP-10)/CXCL10. Thus, the viral vectors were not suitable for this study since the complete removal of plasmids or bacteria-derived contaminants from the preparation of viral vectors was difficult [23]. The advantage of XMRV is that the plasmid-free viral preparation is achievable using 22RV-1 cells latently infected with XMRV [24]. The mouse mammary tumor virus (MMTV) activates the signal from TLR4 that targets non-nucleic acid components [25]. The signals from TLR7, 8, and 9 have been activated by retroviruses [7–12]. Another advantage of using the LNCaP-XMRV system is that LNCaP cells do not express TLR4, 8 and 9, in addition to TLR7 [19]. Furthermore, RNase L and JAK in LNCaP cells are defective, both are involved in the interferon (IFN)-mediated anti-viral responses [26–29]. Thus, the signal we detected was not due to any retroviral sensors identified thus far that target non-nucleic acid components. We chose IP-10/CXCL10, one of the PRR-inducible cytokines, as a marker to monitor the cellular response toward TLR3 ligand according to Galli et al. [19] for the induction of IP-10/CXCL10 by TLR3 ligand was reproducible (Fig. 1B). The replication kinetics of XMRV were measured in relation to the production of IP-10/CXCL10. The IP-10/CXCL10 production profile was almost identical

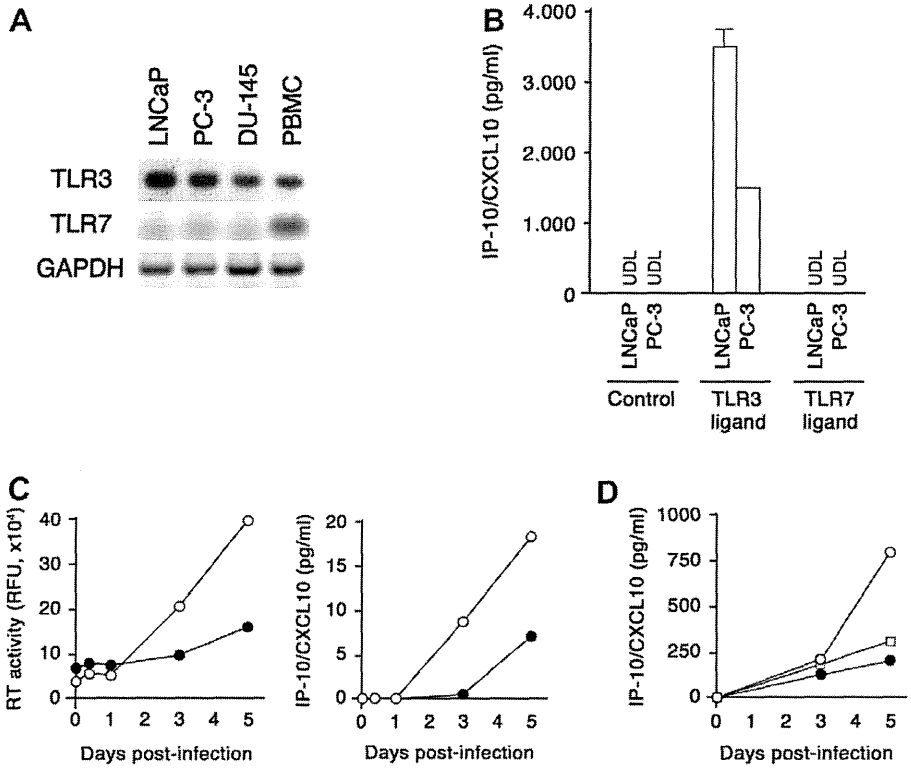

Fig. 1. Expression profiling of TLR3/7 and IP-10/CXCL10 in prostate cancer cell lines. (A) Verification of TLR3 expression in LNCaP, PC-3, and DU-145 cell but not TLR7 by RT-PCR. Total RNA isolated from peripheral blood mononucler cells (PBMC) was used as a positive control. (B) Production of IP-10/CXCL10 in response to TLR3 and TLR7 ligands. LNCaP and PC-3 cells were exposed to TLR3 ligand or TLR7 ligand for 5 days, and the tissue culture supernatants were examined by ELISA. The control is solvent only (PBS and DMSO for TLR3 and TLR7 ligands, respectively). The error bar represents the SD of triplicated wells. Representative data from three independent experiments are shown. UDL, under the detection limit. (C) Correlation of XMRV replication and IP-10/CXCL10 production kinetics in LNCaP cells. The culture supernatant was subjected to RT assay (left) and IP10/CXCL10 ELISA (right). For the control, the replication of XMRV was inhibited by 5 μM AZT (filled). Representative data from three independent experiments are shown. RFU, relative fluorescent units. (D) Induction of IP-10/CXCL10 by XMRV infection in PC-3 cells. Cells were infected with XMRV and maintained in the absence (open circle) or presence (filled circle) of AZT. The MOCK control was also shown (open rectangle).

to the replication profile of XMRV (Fig. 1C). The production of IP-10/CXCL10 from LNCaP cells was reduced when XMRV replication was inhibited by azidothymidine (AZT). Similar results were obtained in PC-3 cells (Fig. 1D). The upregulation of IP-10/CXCL10 was at the transcriptional levels as demonstrated below. These data indicate that XMRV replication induces the expression of IP-10/CXCL10 under the TLR7-null conditions. Note that the IP-10/CXCL10 levels in TLR3 ligand-exposed LNCaP cells were higher than those in XMRV-infected cells (Fig. 1B v.s. Fig. 1C). This is likely because almost all the cells were fully activated by the TLR3 ligand, whereas XMRV infection was limited to a portion of cells.

We then asked whether TLR3 is responsible for these responses. The specific involvement of TLR3 in the upregulation of IP-10/CXCL10 by XMRV infection was investigated by both genetic and chemical approaches. The RNA silencing approach was not employed because siRNA/shRNA potentially serves as a TLR3 ligand [3,30]. First, a dominant-negative derivative of TLR3 (dnTLR3) [31], devoid of cytoplasmic Toll/IL-1 receptor (TIR) domain required for TLR3 signaling, was transduced into LNCaP cells by a murine leukemia virus (MuLV) vector. We verified dnTLR3 expression in LNCaP cells by Western blot analysis where the dnTLR3 was tagged with a HA epitope tag (Fig. 2A). The baseline of the IP-10/CXCL10 production levels was increased in puromycin-selected LNCaP cells. It was assumed that puromycin triggers production of IP-10/CXCL10 since the removal of puromycin from the culture medium reduced the IP-10/CXCL10 levels (data not shown). The control cells responded to both TLR3 ligand and XMRV infection to produce IP-10/CXCL10 (Fig. 2A). In contrast, both XMRV infection and the TLR3 ligand did not upregulate the expression of IP-10/CXCL10 in LNCaP/dnTLR3 cells (Fig. 2A). Second, we treated LNCaP cells with a TLR3 inhibitor and infected cells with XMRV [16]. RT-PCR was employed to examine whether the induction of IP-10/CXCL10 by XMRV infection was at the transcriptional level. Under the conditions whereby the solvent control did not affect the induction of IP-10/CXCL10 by XMRV infection, TLR3 inhibitor was shown to limit the induction of IP-10/CXCL10 by XMRV infection from LNCaP cells (Fig. 2B). The inhibition of IP-10/CXCL10 induction by XMRV was dose-dependent (Fig. 2B). These data suggest that the induction of IP-10/CXCL10 by XMRV infection occurs at the transcriptional level. Taken together, it is suggested that TLR3 is responsible for the recognition of XMRV to induce production of IP-10/CXCL10.

It has been reported that HIV-1 activates TLR7-mediated signals but the contribution of TLR3, a double-stranded RNA sensor in the endosome and on the cell surface, in the anti-retroviral response has remained elusive [7–11]. We demonstrated that not only TLR7 but also TLR3 is able to recognize the retroviral genome and evokes an anti-viral response using XMRV as a model. Retrovirus has a single-stranded RNA as a genome. The retroviral RNA is predicted to form a higher order structure by base-pairing [13–15]. Thus, a portion of retroviral RNA should be able to serve as a TLR3 ligand. Although XMRV was employed in this experiment, it is likely that the recognition of retroviral genome via TLR3 applies to retroviruses in general, including HIV-1. We favor the model that XMRV activates TLR3 signaling at the endosomes given that a similar mechanism has been implicated in the recognition of HIV-1 and HTLV-1 by TLR7 [8,9,11,12]. XMRV has been shown to enter cells via endocytosis [32]. However, some viruses may fail